Atmos. Chem. Phys. Discuss., https://doi.org/10.5194/acp-2017-1072
Manuscript under review for journal Atmos. Chem. Phys.
Discussion started: 30 November 2017

Atmospheric Chemistry and Physics Discussions

Sensitivities of modelled water vapour in the lower stratosphere: temperature uncertainty, effects of horizontal transport and small-scale mixing

Liubov Poshyvailo, Rolf Müller, Paul Konopka, Gebhard Günther, Martin Riese, and Felix Ploeger
Institute of Energy and Climate Research: Stratosphere (IEK-7), Forschungszentrum Jülich, Jülich, Germany.
Correspondence to: Liubov Poshyvailo (l.poshyvailo@fz-juelich.de)

Abstract. Water vapour (H_2O) in the upper troposphere and lower stratosphere (UTLS) is a key player for global radiation. A realistic representation of H_2O is critical for climate model predictions of future climate change. Here, we investigate the effects of current uncertainties in tropopause temperature, horizontal transport and small-scale mixing on simulated H_2O in the lower stratosphere (LS).

To assess the sensitivities of simulated H_2O, we use the Chemical Lagrangian Model of the Stratosphere (CLaMS). First, we examine CLaMS driven by two different reanalysis, ERA-Interim and Japanese 55-year (JRA-55) reanalysis, to investigate the robustness with respect to the meteorological dataset. Second, we carry out CLaMS simulations with transport barriers along latitude circles (at the equator, 15°N/S and 35°N/S) to assess the effects of horizontal transport. Third, we vary the strength of parametrized small-scale mixing in CLaMS.

Our results show significant differences (about 0.5 ppmv) in simulated stratospheric H_2O due to uncertainties in the tropical tropopause temperatures between current reanalysis datasets. The JRA-55 based simulation is significantly moister when compared to ERA-Interim, due to a warmer tropical tropopause in JRA-55 reanalysis. The transport barrier experiments demonstrate that the Northern Hemisphere (NH) subtropics have a strong moistening effect on global stratospheric H_2O. Interhemispheric exchange shows only a very weak effect on stratospheric H_2O. Small-scale mixing mainly increases troposphere-stratosphere exchange, causing an enhancement of stratospheric H_2O, particularly along the subtropical jets and in the Asian monsoon region.

The sensitivity studies presented here provide new insights into the leading processes that control stratospheric H_2O, important for assessing and improving climate model projections.

1 Introduction

Stratospheric water vapour (H_2O) is a crucial factor for global radiation, as it cools the stratosphere and warms the troposphere (e.g., Dessler et al., 2013; Forster and Shine, 1999, 2002). Particularly, changes in H_2O mixing ratios in the upper troposphere and lower stratosphere (UTLS) may have significant effects on climate variability (Solomon et al., 2010; Riese et al., 2012; Maycock et al., 2013). Thus, the reliability of climate model predictions is significantly affected by the representation of the processes controlling the distribution of stratospheric H_2O. However, there is a multitude of such critical processes, poorly

Atmos. Chem. Phys. Discuss., https://doi.org/10.5194/acp-2017-1072
Manuscript under review for journal Atmos. Chem. Phys.
Discussion started: 30 November 2017

Atmospheric Chemistry and Physics Discussions

Simulation type	Abbreviation	Reanalysis dataset	Latitude barriers	Mixing strength (λ_c, day^{-1})
Reference	REF	ERA-Interim	–	1.5
Reanalysis uncertainty	JRA-55	JRA-55	–	1.5
Horizontal transport effects	BAR-0	ERA-Interim	5° S - 5° N	1.5
	BAR-15	ERA-Interim	10° S - 20° S, 10° N - 20° N	1.5
	BAR-15S	ERA-Interim	10° S - 20° S	1.5
	BAR-15N	ERA-Interim	10° N - 20° N	1.5
	BAR-35	ERA-Interim	30° S - 40° S, 30° N - 40° N	1.5
Small-scale mixing effects	MIX-no	ERA-Interim	–	0.0
	MIX-weak	ERA-Interim	–	2.0
	MIX-strong	ERA-Interim	–	1.0

Table 1. CLaMS sensitivity simulations with respect to the used reanalysis datasets, horizontal transport barriers and small-scale mixing strength.

understood and quantified hitherto, rendering the representation of stratospheric H_2O a major uncertainty factor for global climate models (Gettelman et al., 2010; Randel and Jensen, 2013).

A critical region for the control of H_2O entering the stratosphere is the tropical tropopause layer (TTL) (Fueglistaler et al., 2009), extending from the level of main convective outflow around 12 km up to altitudes around 18 km (the highest level convection may reach). The TTL has physical and chemical characteristics midway between the troposphere and stratosphere. Because the TTL is a region of mean upward transport it acts as a "gate to the stratosphere" for trace species and pollution with sources in the troposphere.

Transport processes in the TTL are rather complex, involving large-scale upwelling and horizontal advection linked to the residual mean mass circulation, but also large-scale horizontal and small-scale vertical mixing processes. These mixing processes are particularly important during boreal summer, when mass transport related to the residual circulation is weak. Vertical mixing has been shown to affect trace gas transport in the tropical LS (e.g., Mote et al., 1998; Glanville and Birner, 2017). Horizontal transport between the TTL and middle latitudes is strongly influenced by the Asian monsoon anticyclone and other subtropical circulation systems. Rapid transport from the tropics to middle latitudes occurs mostly above the subtropical jets within the "tropically controlled transition region" (Rosenlof et al., 1997).

Related to the mean upward transport, the TTL includes the region of very low temperatures around the cold-point tropopause, where the moist tropospheric air is freeze-dried to the low stratospheric values (Brewer, 1949). The dehydration occurs as a result of the slow upward and large-scale horizontal motion of air in this region (Holton and Gettelman, 2001). The freezing is sensitive not just to TTL temperatures, but also to microphysical processes controlling the ice crystal number densities, particle size distribution, and fall speed (Hardiman et al., 2015).

Atmos. Chem. Phys. Discuss., https://doi.org/10.5194/acp-2017-1072
Manuscript under review for journal Atmos. Chem. Phys.
Discussion started: 30 November 2017

Atmospheric Chemistry and Physics Discussions

Sublimation of ice, injected by deep convection, has also been argued to be an important factor for the H_2O budget of the tropical lower stratosphere (e.g., Avery et al., 2017). Although from a microphysical perspective, the freezing process is rather complex. The tropical stratospheric entry H_2O mixing ratios can be well simulated by the advection through the large-scale temperature field and instantaneous freezing, often described as the "advection-condensation" paradigm (Pierrehumbert and Rocca, 1998; Fueglistaler and Haynes, 2005). However, based on trajectory studies driven by ECMWF reanalysis Liu et al. (2011) showed that such results are largely sensitive to the temperature and vertical velocity fields.

The annual cycle of TTL temperatures (minimum in boreal winter, maximum in summer) is imprinted on H_2O mixing ratios entering the stratosphere, forming the so-called "tape recorder" signal (Mote et al., 1995, 1996). The summer maximum of tropical H_2O mixing ratios is in addition related, to some degree, to the subtropical monsoon circulations like the Asian monsoon. However, the strength of this effect is a matter of debate (Bannister et al., 2004; James et al., 2008; Wright et al., 2011; Randel and Jensen, 2013).

Satellite observations suggest that horizontal transport from low latitudes affects the H_2O distribution in middle and high latitudes (Rosenlof et al., 1997; Pan et al., 1997; Randel et al., 2001). Additionally, model simulations confirmed that almost the entire annual cycle of H_2O mixing ratios in the Northern Hemisphere (NH) extratropical LS above about 360 K, with maximum mixing ratios during summer and fall, is caused by horizontal transport from low latitudes (Ploeger et al., 2013). In the respective model, highest H_2O mixing ratios in this region are clearly linked to horizontal transport from low latitudes, mainly from the Asian monsoon.

Above the TTL, H_2O behaves mainly as a tracer, and the tape recorder signal imprinted at the cold-point tropopause ascends deep into the tropical stratosphere (Mote et al., 1996). At higher altitudes in the stratosphere, methane oxidation results in a chemical source for stratospheric H_2O (e.g., LeTexier et al., 1988; Rohs et al., 2006). As a net result of this oxidation process each methane molecule is converted into approximately two H_2O molecules. Hence, the total water vapour (TWV), $TWV = 2CH_4 + H_2O$, is unchanged by transport in the stratosphere and can be regarded approximately constant, where CH_4 is a mixing ratio of methane (e.g., Dessler et al., 1994; Mote et al., 1998; Randel et al., 1998). Therefore, the sum $2CH_4 + H_2O$ is an important value to indicate the amount of water entering the stratosphere (e.g., Kämpfer, 2013).

Based on model simulations Riese et al. (2012) have shown that little changes in small-scale mixing, which may be related to deformations in the large-scale flow, cause strong effects on the H_2O distribution in the LS. Consequently, uncertainties in the representation of small-scale characteristics of transport in the LS in models may cause substantial uncertainties in the stratospheric H_2O distribution. This, in turn causes uncertainties in the simulated radiative effect of H_2O and of surface temperatures.

In summary, stratospheric H_2O mixing ratios are a result of the interplay of a multitude of complex processes. As these various processes are influenced by climate change in different ways, long-term changes of stratospheric H_2O are complicated to interpret (e.g., Hegglin et al., 2014) and to predict (e.g., Gettelman et al., 2010). In this paper, we investigate uncertainties of modelling H_2O in the LS with respect to the meteorological datasets used to drive transport and freeze-drying, horizontal transport between tropics and extratropics and small-scale mixing. For that reason, we carried out a number of sensitivity simulations with CLaMS (see Table 1). Our main results show a significant uncertainty for modelling stratospheric H_2O with

respect to the underlying meteorological data (in particular TTL temperatures), even when the most current reanalysis products are used. Furthermore, we find a substantial effect of horizontal transport to moisten the tropical LS and to dry the extratropics. The NH subtropics turn out to be a major moisture source region for the global stratosphere. Finally, small-scale mixing has a strong effect on stratospheric H_2O, by increasing diffusive cross-tropopause moisture transport and horizontal mixing in the stratosphere.

The model and datasets which were used, as well as the various sensitivity simulations, are described in Section 2. The results regarding different reanalysis, horizontal transport and small-scale mixing are presented in Section 3. A discussion of the results is presented in Section 4.

2 Method

2.1 The CLaMS model and simulation set-up

We carried out a number of sensitivity simulations using the Chemical Lagrangian Model CLaMS (McKenna et al., 2002a, b) in its 3D-version (Konopka et al., 2004). CLaMS is a Lagrangian transport model based on 3D-forward trajectories and an additional parametrization of small-scale mixing. The time-dependent irregular model grid is defined by Lagrangian air parcels, which follow the flow. An advantage of the Lagrangian approach for simulating stratospheric transport is the ability to resolve small-scale features, which are often below the possible resolution of high-resolved Eulerian models (McKenna et al., 2002b). Such small-scale features are frequently observed in stratospheric trace gas distributions as elongated filaments, related to the stretching and differential advection in sheared flows (Orsolini et al., 1998).

The advection of forward trajectories in CLaMS is calculated based on a fourth-order Runge-Kutta scheme, as described by McKenna et al. (2002a), using 6-hourly wind fields from meteorological reanalysis data. For vertical transport, CLaMS uses a hybrid vertical coordinate, which is an orography-following σ-coordinate at the ground and transforming into potential temperature above (Mahowald et al., 2002; Pommrich et al., 2014). Above $\sigma = 0.3$ (about 300 hPa), the vertical coordinate is purely isentropic, and vertical transport is driven by the reanalysis total diabatic heating rate (Ploeger et al., 2010). For the simulations considered here we use a horizontal resolution of about 100 km. The vertical resolution is defined via a critical aspect ratio α of 250 (Haynes and Anglade, 1997). This value expresses the ratio between horizontal and vertical scales, and is about 400 m around the tropical tropopause, degrading below and above it (Konopka et al., 2012). The simulations cover the atmosphere from the surface to about the stratopause, and the number of air parcels advected in the simulations is around 2 millions at each time step.

The parametrization of small-scale mixing in CLaMS is based on the deformation rate in the large-scale flow. Hence, air parcels may be merged, or new air parcels may be inserted at each time step (every 24 h), depending on the critical distances between them. The strength of parametrized small-scale mixing can be controlled by choice of a critical finite-time Lyapunov exponent, λ_c (for details see McKenna et al., 2002a; Konopka et al., 2004).

Stratospheric H_2O in CLaMS is calculated using the CLaMS cirrus module. It includes freeze-drying in regions of cold temperatures, which mainly occurs around the tropical tropopause (dehydration). This, in turn, causes formation and sedimen-

Atmos. Chem. Phys. Discuss., https://doi.org/10.5194/acp-2017-1072
Manuscript under review for journal Atmos. Chem. Phys.
Discussion started: 30 November 2017

Atmospheric Chemistry and Physics Discussions

tation of ice particles. If saturation along a CLaMS air parcel trajectory exceeds a critical saturation (100% with respect to ice), then the H_2O amount in excess is instantaneously transformed to the ice phase and partly sediments out. Such simple parametrisation has been adopted in several global Lagrangian studies (e.g., Kremser et al., 2009; Stenke et al., 2008). The saturation mixing ratio is calculated as $\chi_{H_2O} = p_s/p_{cold\_point}$ for each air parcel trajectory, with the saturation pressure given by $p_s = 10^{-2663.5/T+12.537}$ (Marti and Mauersberger, 1993), where p_{cold_point} is the ambient pressure (e.g., Kremser et al., 2009).

For sedimentation, a parametrization is based on a mean ice particle radius, a characteristic sedimentation length and the corresponding fall speed. When the fallen path of the ice particles is calculated from the fall speed and the computation time step Δt, it is compared with a characteristic sedimentation length of about the vertical grid size (here $l_c = 300\,m$) which has been empirically optimized by comparison with observations (Ploeger et al., 2013). After this step a respective fraction of ice will be removed. If the parcel is sub-saturated and ice exists, this ice is instantaneously evaporated to maintain saturation.

In addition, methane oxidation is included as a source of H_2O in the middle and upper stratosphere. Therefore, hydroxyl, atomic oxygen, and chlorine radicals are taken from a model climatology (for details see Pommrich et al., 2014).

To study the sensitivity of simulated stratospheric H_2O regarding different reanalysis temperatures, horizontal transport effects and small-scale mixing, we carried out several CLaMS simulations. As a reference, we consider the run driven by ERA-Interim reanalysis data (Dee et al., 2011). To reach steady state we use a perpetuum technique, where the one year run (for 2011 conditions) is repeated several times. The initial values for the tracer fields at the first day of the simulation are taken from a long-term CLaMS simulation (Pommrich et al., 2014). After one year of the perpetuum calculation, tracer mixing ratios from the 31st of December 2011 are interpolated to the air parcel positions on 1st of January 2011, and the calculation is repeated for 2011 again. After the fourth year, the maximum relative change of H_2O mixing ratios is very small (below 0.75 %, see Table 2). Thus, we use the fifth year of the perpetuum simulation for our further analysis. Restricting the analysis to a single year, instead of calculating a multi-year climatology, has no effect on our conclusions regarding the differences between different simulations, as shown in Appendix A.

n, n + 1	$\frac{\lvert H_2O^{(n)} - H_2O^{(n+1)} \rvert}{H_2O^{(n)}}$, %
PR0, PR1	5.64744
PR1, PR2	2.68264
PR2, PR3	1.42625
PR3, PR4	0.751254
PR4, PR5	0.435446
PR5, PR6	0.253376
PR6, PR7	0.148043
PR7, PR8	0.086229

Table 2. The maximal relative differences of H_2O volume mixing ratio between perpetuum simulations in the model domain ranging from the surface to the stratopause; *n* is the number of the perpetuum cycle.

Atmos. Chem. Phys. Discuss., https://doi.org/10.5194/acp-2017-1072
Manuscript under review for journal Atmos. Chem. Phys.
Discussion started: 30 November 2017

Atmospheric Chemistry and Physics Discussions

First, to assess the robustness of simulated H_2O with respect to the meteorological datasets we carry out another CLaMS simulation driven by the Japanese 55-year reanalysis data (JRA-55) (Kobayashi et al., 2015), and compare it to the ERA-Interim based reference simulation.

Second, to assess the effects of horizontal transport, we carry out sensitivity simulations with horizontal transport barriers along latitude circles at the equator, at 15°N/S and at 35°N/S (Ploeger et al., 2013). The transport barriers are defined in the model and centred at the given latitude. Their thickness is 10° in latitude (to inhibit diffusive mixing transport), and the barriers extend from the ground to 600 K potential temperature. Air parcels entering the barrier along their trajectories during one model time step are moved to their starting locations after Δt, as shown in Figure 1. Air parcels which were mixed into the barrier after the mixing procedure are moved to the closer barrier edge after the time step. Because of the broad barrier width of 10°, this technique inhibits all cross-barrier transport. The CLaMS mixing parametrization ensures that no unrealistic clustering of air parcels occurs at the barrier edges.

Third, to investigate the effects of small-scale mixing, we vary the parametrized mixing strength in CLaMS. A discussion of the choice of the critical Lyapunov coefficient, controlling the strength of small-scale mixing in CLaMS, is given by Riese et al. (2012); Konopka et al. (2005). Hence, for a horizontal resolution of 100 km and a mixing step of 24 h, which were used also in our studying, Lyapunov coefficients of 1.5 day^{-1} and 1.2 day^{-1} provide good agreement between observations and simulation results. Even for such a small difference in the small-scale mixing strengths, H_2O concentrations in the extra-tropical LS differs

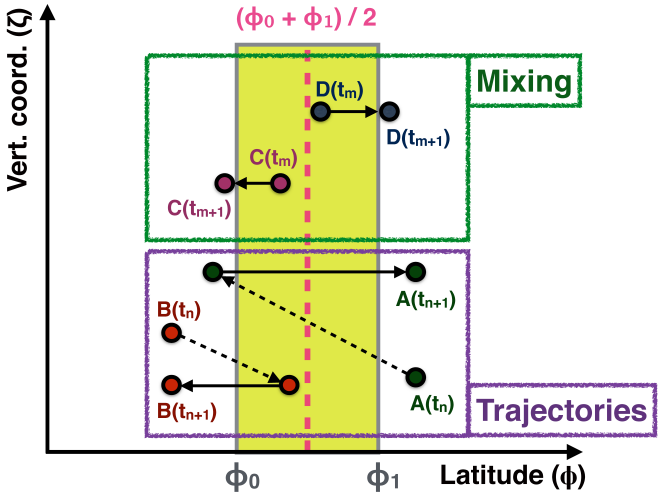

Figure 1. A schematic of the implementation of transport barriers in the CLaMS model into the trajectory and mixing modules respectively. The x-axis represents latitude, the y-axis is the vertical coordinate, respectively. The barrier is shown in light-green colour, between ϕ_0 and ϕ_1 latitudes. The capital letters A, B, C and D represent the cross-barrier movements of different air parcels between time steps t_n and t_{n+1} for the trajectory module, and t_m and t_{m+1} for the mixing module.

Atmos. Chem. Phys. Discuss., https://doi.org/10.5194/acp-2017-1072
Manuscript under review for journal Atmos. Chem. Phys.
Discussion started: 30 November 2017

by about 10-15% (Riese et al., 2012; McKenna et al., 2002a). Furthermore, Konopka et al. (2004, 2005) showed that the value of $\lambda_c = 1.5\,day^{-1}$ for the chosen horizontal resolution and time step here, turns out to be optimal for the 3D version of CLaMS.

In our study we use a value of $\lambda_c = 1.5\,day^{-1}$ for the reference run, $2.0\,\mathrm{day}^{-1}$ to represent weak mixing, and $1.0\,\mathrm{day}^{-1}$ for modelling strong mixing. Furthermore, we carry out a simulation without small-scale mixing (mixing in CLaMS was switched off). The large range of chosen mixing parameters here (λ_c) enables investigating sensitivities throughout a large range of possible mixing strengths, even including significantly changed mixing characteristics in potential future climate.

Note again that small-scale mixing in CLaMS is parametrized in a physical way, by coupling the mixing intensity to deformations in the large-scale flow. The sensitivity of simulated H_2O to the parametrized mixing strength can therefore be regarded representative to the response of changes in small-scale turbulence, as well as to the response of changes in numerical diffusion in climate models.

2.2 Satellite observations

We use satellite observations from Microwave Limb Sounder (MLS) and Atmospheric Chemistry Experiment-Fourier Transform Spectrometer (ACE-FTS) for validation of the CLaMS simulations. For MLS, we use Level 2 data of Version 4. Detailed information on the MLS instrument can be found in Waters et al. (2004), and a general discussion of the microwave sounding technique is given in Waters et al. (1999). The MLS instrument was launched on 15 July 2004 on the NASA Aura satellite and measured limb emissions in broad spectral regions. Vertical profiles are retrieved every 165 km along the suborbital track, covering 82° S to 82° N latitudes on each orbit. Generally, MLS measurements include around 15 atmospheric chemical species along with temperature geopotential height, relative humidity (deduced from the H_2O and temperature data), cloud ice water content and cloud ice water path, all described as functions of pressure. All measurements are made simultaneously and continuously, during both day and night (Waters et al., 2006). The resolution of the retrieved data is strictly related to the averaging kernels (Rodgers, 2000), which describe both vertical and horizontal resolution. Particularly, the vertical resolution for H_2O is around 3 km in the UTLS region, whereas the along-track horizontal resolution is in between 170 and 350 km (Livesey et al., 2017).

As a second satellite observation we used ACE-FTS Version 3.6. ACE-FTS is a part of a Canadian satellite mission for remote sensing of the Earth's atmosphere, SCISAT, which was launched into low Earth circular orbit on 12th of August 2003. ACE-FTS is a satellite instrument which covers the spectral region from 750 to $4400\,cm^{-1}$, and works mainly in solar occultation. During sunrise and sunset, the ACE-FTS instrument measures sequences of atmospheric absorption spectra in the limb viewing geometry. Further, the spectra are analysed and inverted into vertical profiles. Aerosols and clouds are being monitored using the extinction of solar radiation. The satellite provides altitude profile information (typically from 10 to 100 km) for temperature, pressure, and the volume mixing ratios for several molecule species over the latitudes from 85° N to 85° S (Bernath et al., 2005). Solar occultation instruments like the ACE-FTS could have a high vertical resolution as good as ≈ 1 km, but low horizontal resolution (≈ 300 km) in the limb direction (Hegglin et al., 2008). A detailed description of ACE-FTS is given by Bernath (2017).

Atmos. Chem. Phys. Discuss., https://doi.org/10.5194/acp-2017-1072
Manuscript under review for journal Atmos. Chem. Phys.
Discussion started: 30 November 2017

Atmospheric Chemistry and Physics Discussions

Hurst et al. (2016) compare MLS lower stratospheric H_2O observations with balloon-borne Cryogenic Frostpoint Hygrometer (CFH) and Frost Point Hygrometer (FPH) instruments, from 2004 to 2015. There is a potential drift between the two sets of measurements, with MLS H_2O increasing at a rate of around 0.03-0.07 ppmv yr^{-1} relative to the hygrometer measurements, starting around 2009. In contrast, the comparisons with recent ACE-FTS data show no signs of such drift in MLS H_2O, nor do comparisons of MLS upper stratospheric H_2O with ground-based microwave measurements (Livesey et al., 2017).

3 Results

Figure 2 shows the annual cycle of tropical entry of H_2O at 400 K for all simulations. While a clear annual cycle is evident for all cases, the mixing ratios vary by more than 1 ppmv between the simulations. The reference simulation (REF) agrees well with MLS data, although there are some small differences during boreal winter. The impact of horizontal transport sensitivity simulations is slightly higher than for the small-scale mixing. However, this depends on the range of mixing strength covered. The largest sensitivity (spread between simulations) occurs for boreal summer and fall months. Suppressing horizontal transport from the subtropics into the tropics (BAR-15) significantly dries the tropical entry H_2O, with difference to the reference of up to around 1 ppmv. For the mixing sensitivity simulations, the largest difference from the reference case occurs for the case without mixing (MIX-no) and reaches the values of $\approx$ 0.8 ppmv. The CLaMS simulation driven with JRA-55 shows moister values in the TTL compared to the ERA-Interim simulation.

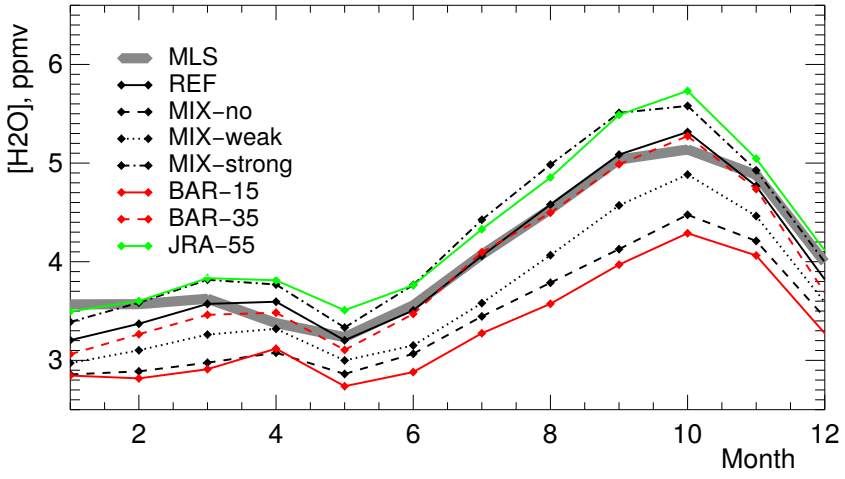

Figure 2. Annual cycle of tropical entry H_2O at 400 K (10°S-10°N) from different sensitivity simulations with respect to variations in reanalysis datasets, horizontal transport and small-scale mixing. Grey line represents MLS satellite observations, for comparison. Shown are the reference simulation (REF), the cases without mixing (MIX-no), with weak (MIX-weak) and strong mixing (MIX-strong), the simulations with transport barriers at 15°S/15°N (BAR-15), at 35°S/35°N (BAR-35), and the simulation driven with JRA-55 reanalysis data (JRA-55).

Atmos. Chem. Phys. Discuss., https://doi.org/10.5194/acp-2017-1072
Manuscript under review for journal Atmos. Chem. Phys.
Discussion started: 30 November 2017

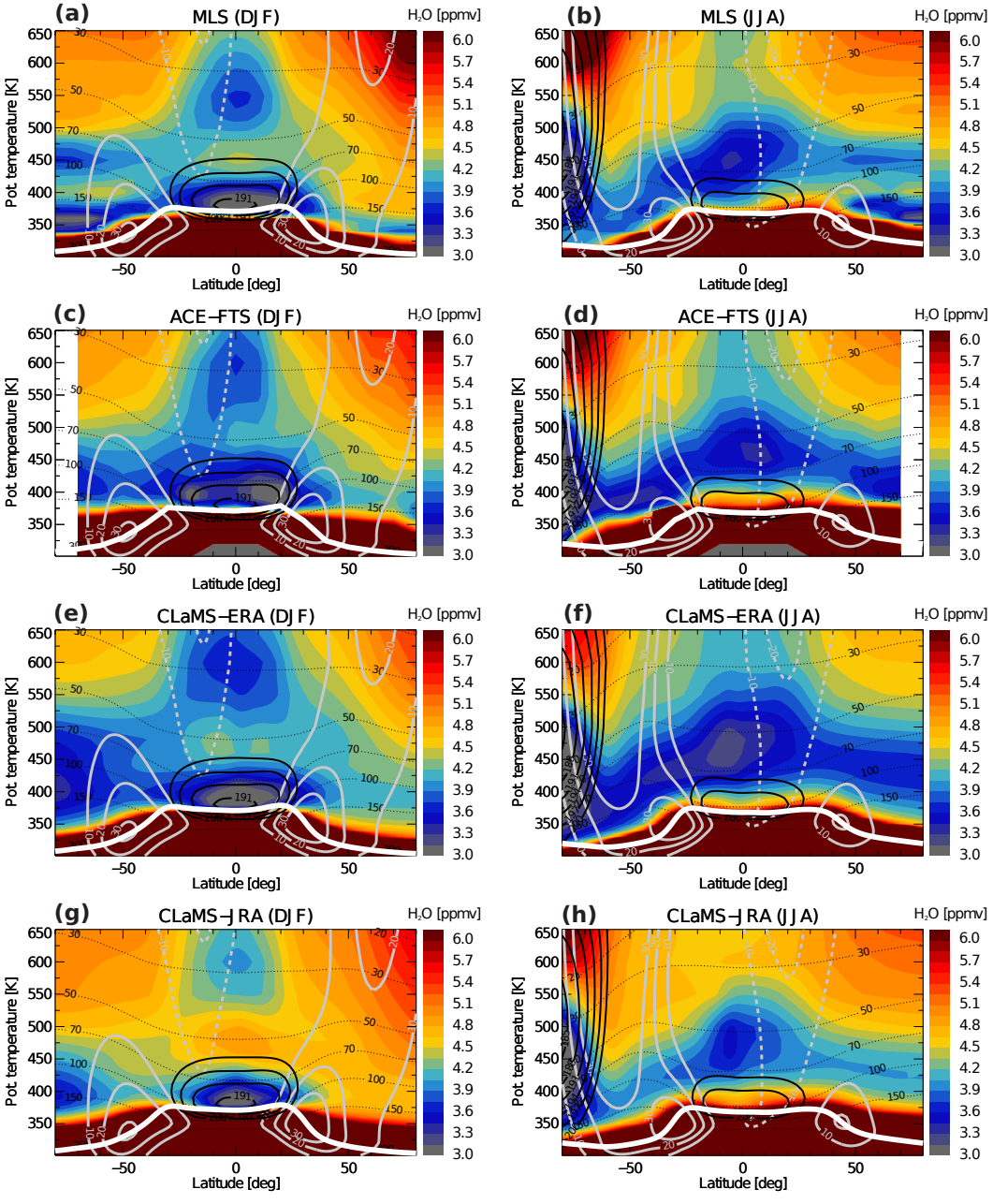

Figure 3. Zonal mean H_2O distributions for winter (DJF, left) and summer (JJA, right) from MLS and ACE-FTS satellite observations, as well as for CLaMS simulations driven with either ERA-Interim or JRA-55 reanalysis. Data shown are climatologies for 2004-2013 years. Black contours show temperatures (185 K, 188 K, 191 K, 194 K, 197 K, 200 K), grey contours are zonal winds (10 m/sec, 20 m/sec, 30 m/sec), black dotted lines are pressure levels (in hPa) and the white line is the thermal tropopause.

Atmos. Chem. Phys. Discuss., https://doi.org/10.5194/acp-2017-1072
Manuscript under review for journal Atmos. Chem. Phys.
Discussion started: 30 November 2017

Atmospheric Chemistry and Physics Discussions

The strong sensitivity of tropical entry H_2O shows that the TTL temperatures from the used reanalysis dataset, horizontal transport and small-scale mixing are critical control factors for stratospheric H_2O. They will be investigated in more detail, in the following.

3.1 Reanalysis uncertainty

Zonal mean H_2O mixing ratios for boreal winter (December-February, DJF) and summer (June-August, JJA) from MLS and ACE-FTS satellite observations, and from CLaMS simulations driven by ERA-Interim and JRA-55 are shown in Figure 3. The comparison of the two different satellite datasets (first and second row) shows differences of about 0.5 ppmv (with ACE-FTS being moister), and even larger in the extratropical LS. Oscillations in MLS H_2O at high latitudes are a known effect of the broad averaging kernel (Ploeger et al., 2013).

Comparison between the two simulations, driven by either ERA-Interim and JRA-55 (third and fourth row), shows differences due to the used reanalysis dataset of about 0.5 ppmv, increasing towards the extratropical lowermost stratosphere. The main reason for JRA-55 causing a moister stratosphere, when compared to ERA-Interim is the positive difference in the temperatures around the TTL (Fig. 4). Zonal mean temperatures in this region are on average about 2 K higher for JRA-55 than for ERA-Interim. Remarkably, these differences only exist in a narrow layer around the tropical tropopause. In addition to temperature, also differences in winds and heating rates between the two reanalyses could cause differences in H_2O mixing ratios, however, the temperature difference provides a self-evident explanation.

A detailed comparison of LS H_2O between MLS and ERA-JRA-driven CLaMS simulations at 380 K is given in Figure 5. The patterns of dominant freeze-drying regions above the West Pacific and South America in boreal winter are consistent between the observations and the two simulations. Notably, the larger area of low H_2O mixing ratios and colder temperatures for ERA-Interim when compared to JRA-55, is consistent with the drier global stratosphere, as discussed above. Also in boreal

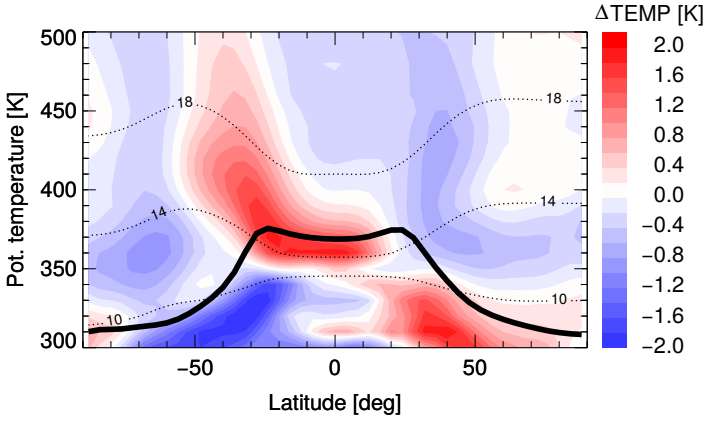

Figure 4. Differences in the zonal mean temperatures between JRA-55 and ERA-Interim reanalysis data averaged for the period of 1979-2013; black dotted lines are altitude levels (in km) and the black line is the thermal tropopause.

Atmos. Chem. Phys. Discuss., https://doi.org/10.5194/acp-2017-1072
Manuscript under review for journal Atmos. Chem. Phys.
Discussion started: 30 November 2017

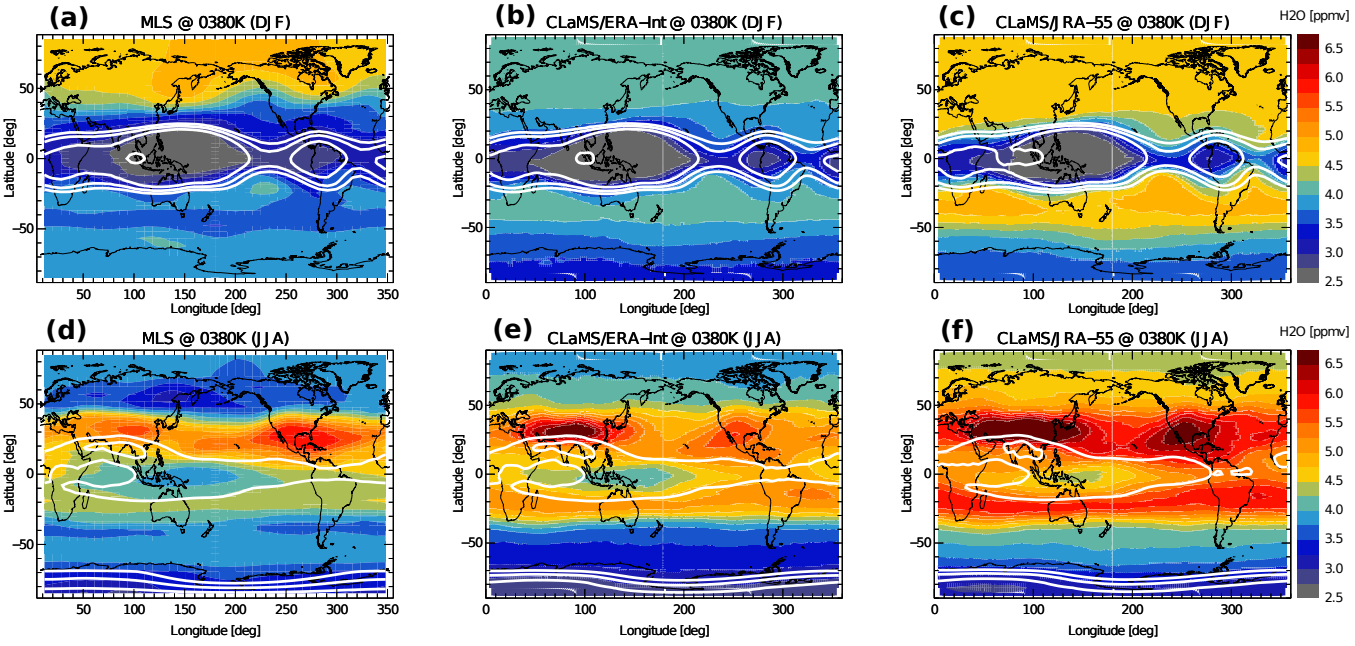

Figure 5. Water vapour maps at 380 K from MLS (a, d), and CLaMS simulations driven by ERA-Interim (b, e) and JRA-55 (c, f). Shown are winter (December-February, DJF) and summer (June-August, JJA) data, respectively, from a 2004-2013 climatology. White lines show temperature contours (191 K, 193 K, 195 K).

summer, the H_2O distributions for MLS observations and CLaMS, driven by the two reanalyses, are similar in the tropics. Nevertheless, in the subtropics, the strength of summer time monsoon anomalies in MLS differs from CLaMS, with the Asian monsoon dominating in both simulations, while the American monsoon appears stronger in MLS data (e.g., Ploeger et al., 2013).

Overall, regarding the global H_2O distributions and maps in the LS, CLaMS modelling results with ERA-Interim are drier when compared to JRA-55, resulting from lower TTL temperatures in ERA-Interim. In fact, these lower ERA-Interim based H_2O mixing ratios appear to agree slightly better with MLS and ACE-FTS observations than JRA-55, especially in the LS region.

3.2 Horizontal transport effects

Probability density functions (PDFs) of H_2O mixing ratio (e.g., Schoeberl et al., 2013), allow a simple comparison of the overall effects of horizontal transport on lower stratospheric H_2O by contrasting the various sensitivity simulations. Figure 6 shows these PDFs for the tropics and extratropics of both hemispheres for the different barrier simulations.

In the tropics, the vanishing difference between the reference (REF) and an equatorial transport barrier (BAR-0) simulations show that the deep tropics (5°S-5°N) are rather unimportant for tropical mean H_2O mixing ratios. Similarly, in-mixing of

Atmos. Chem. Phys. Discuss., https://doi.org/10.5194/acp-2017-1072
Manuscript under review for journal Atmos. Chem. Phys.
Discussion started: 30 November 2017

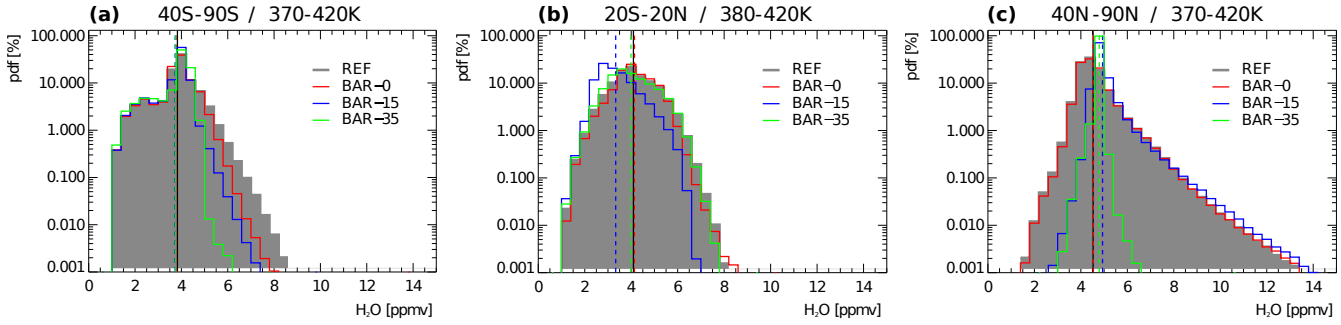

Figure 6. Probability density function (PDF) for water vapour mixing ratios in the SH extratropics for 40°S-90°S between 370 K and 420 K (a), in the tropics for 20°S-20°N between 380 K and 420 K (b), and in the NH extratropics for 40°N-90°N between 370 K and 420 K (c). Shown data are from 2011 CLaMS sensitivity simulations with horizontal barriers along latitude circles at 0° (BAR-0, red solid line), 15° N/S (BAR-15, blue solid line), 35° N/S (BAR-35, green solid line) and the reference (REF, grey background). Dashed coloured lines represent the mean H_2O values for the different simulations respectively, whereas the black solid line shows the mean value of the reference simulation.

mid- and high-latitude air (see BAR-35) has a vanishing effect on tropical mean H_2O, in agreement with the findings of Ploeger et al. (2012). In contrast, transport from the subtropics has a strong effect. Suppressing such transport by applying a barrier changes the PDF substantially, as evident from the difference between the simulation with transport barrier at 15°S/N (BAR-15) and the reference and BAR-35 cases. Without transport from the subtropics, the tropical H_2O PDF appears more strongly skewed against low mixing ratios (blue line in Fig. 6), and the mean H_2O mixing ratio is shifted towards lower values by about 0.5 ppmv.

In the NH (Fig. 6c), cross-equatorial transport from the SH is unimportant, and an equatorial transport barrier has no effect. Introducing a transport barrier in the subtropics at 15°N removes the low mixing ratios from the PDF, showing that these low mixing ratios result from transport out of the deep tropics. Moving the transport barrier further away from the equator to 35°N, changes the PDF drastically. In addition to the low mixing ratios it also removes the tail of the PDF at high mixing ratios, such that a very narrow extratropical H_2O mixing ratio PDF remains. Hence, these high mixing ratios are the result of transport from the subtropics, and are likely related to the Asian monsoon, as argued by Ploeger et al. (2013).

In the SH (Fig. 6a) the frequent very low mixing ratios are insensitive to horizontal transport, indicating the occurrence of local dehydration. This insensitivity reflects the fact that temperatures in the Antarctic polar vortex are so low that H_2O mixing ratios are locally freeze-dried to the saturation value. However, there is a weak effect of transport from the NH on moistening the SH, indicated by a lowering of the PDF's tail without cross-equatorial transport. Suppressing transport from the tropics lowers the tail further, and suppressing transport from the SH subtropics (with the 35°S barrier) finally removes almost all mixing ratios higher than 5 ppmv. Accordingly, monsoon driven H_2O transport from the subtropics to the high latitudes is more pronounced for the NH than for SH.

Atmos. Chem. Phys. Discuss., https://doi.org/10.5194/acp-2017-1072
Manuscript under review for journal Atmos. Chem. Phys.
Discussion started: 30 November 2017

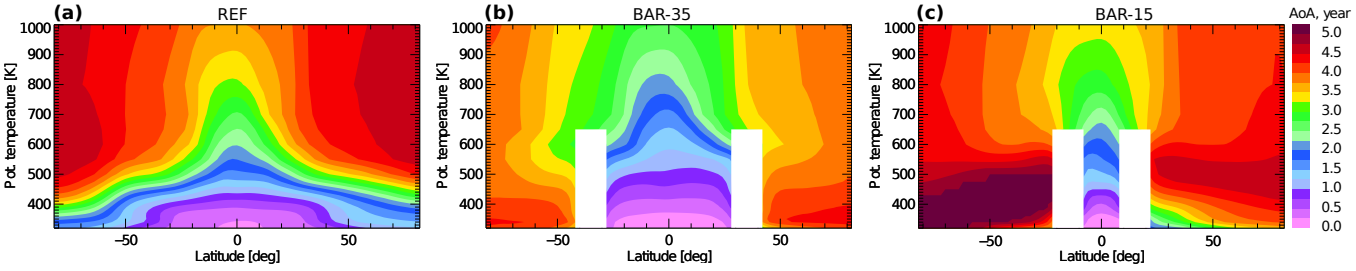

Figure 7. Zonal mean age of air distributions for 2011. Shown data are from CLaMS sensitivity simulations for the reference (a) and the horizontal transport barrier simulations along latitude circles at 35° N/S (b) and 15° N/S (c). Barriers are set between the Earth's surface and the 600 K potential temperature levels and are represented in white.

The pure transport effects of horizontal exchange between tropics and mid-latitudes are evident from mean age of air (AoA), the mean transit time for air through the stratosphere for the different model experiments with horizontal transport barriers. Figure 7 shows CLaMS calculations of the AoA for the reference case (Fig. 7a) and for the simulations with transport barriers in the subtropics at 35° (Fig. 7b) and 15° (Fig. 7c). These tropical and subtropical transport barriers effectively isolate the tropical pipe from the in-mixing of older stratospheric air from mid-latitudes. The clearest effect occurs with transport barriers at 35° significantly decreasing the AoA globally by more than a year. Hence, recirculation from mid-latitudes into the tropics has a strong ageing effect on the stratosphere globally, in agreement with (Neu and Plumb, 1999). Without recirculation (in the BAR-35 simulation) the global AoA distribution reflects mainly the pure effect of the residual circulation, resulting in oldest air in the extratropical lowermost stratosphere, and appears very similar to the distribution of residual circulation transit times (e.g., Ploeger et al., 2015). Older air in the NH is related to the deeper NH residual circulation cell.

In the tropics, the age distribution shows a double peak structure up to about 500 K, indicating that the subtropics are regions of particularly fast transport, likely related to subtropical processes like monsoon circulations. Suppressing transport in the subtropics with barriers between 10°-20° N/S (BAR-15 case) therefore significantly increases AoA in the extra-tropics (Fig. 7c) and, consequently, throughout the global stratosphere. An interesting detail is that the extratropical lower stratosphere (below about 500 K) becomes younger in the NH than in the SH in the BAR-15 simulation. This indicates that transport out of the NH subtropics poleward of 20°N ventilates the NH lower stratosphere, decreasing AoA.

Relating the pure horizontal transport effects seen in age of air to H_2O is not straightforward, as H_2O is strongly controlled by TTL temperatures. Figure 8 shows the annual zonal mean H_2O mixing ratio for the different sensitivity simulations with transport barriers. The small differences between the reference (Fig. 8a) and the equatorial barrier (Fig. 8b) simulations indicate only a very weak effect of transport processes in the deep tropics and interhemispheric exchange on global stratospheric H_2O. Similarly, the sensitivity simulation with a subtropical transport barrier at 35° N/S (Fig. 8c) shows that in-mixing of mid-latitude air has only a weak impact on global stratospheric H_2O (except in the NH lower stratosphere). In contrast, transport from the subtropics, between 10° and 30° S/N, as visible from the comparison of sensitivity simulation BAR-15 and BAR-35 (Fig. 2, 8c, 8d), has a strong effect on tropical entry H_2O and hence on global H_2O. Without such transport from the subtropics,

Atmos. Chem. Phys. Discuss., https://doi.org/10.5194/acp-2017-1072
Manuscript under review for journal Atmos. Chem. Phys.
Discussion started: 30 November 2017

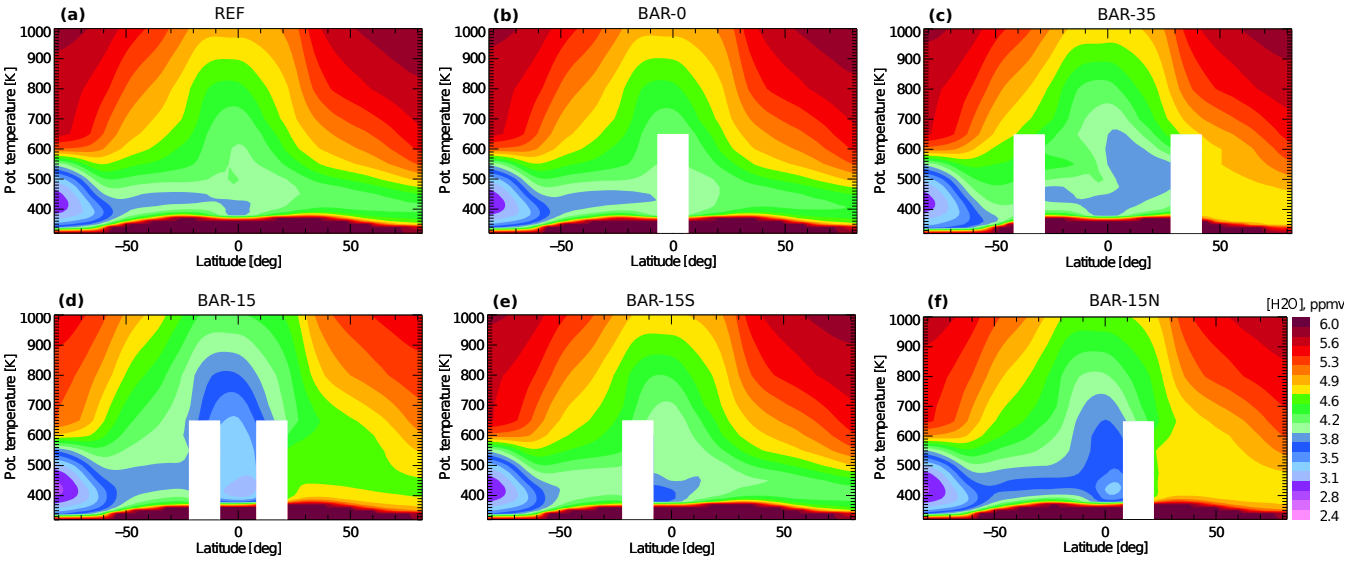

Figure 8. Zonal mean water vapour distributions for 2011. Shown data are from CLaMS sensitivity simulations for the reference (a) and the horizontal transport barrier simulations along latitude circles at 0° (b), 35° N/S (c), 15° N/S (d), 15° S (e) and 15° N (f). Barriers are set between the Earth's surface and the 600 K potential temperature levels and are represented in white.

the global stratosphere becomes substantially drier (up to about 1 ppmv). The fact that this drying occurs only with transport barriers at 15° S/N and not with barriers at 35° S/N, shows that it is not related to the suppression of recirculation of aged air from mid-latitudes, which has been affected by methane oxidation. In fact, processes in the subtropics (e.g., monsoon circulations) have a strong effect in moistening the global stratosphere, and suppressing these processes in BAR-15 causes drying. The model experiments with transport barriers only in the NH or SH subtropics further show that the effect of the NH subtropics in moistening the global stratosphere is much stronger compared to the SH subtropics.

Figure 9 shows the H_2O seasonal cycle at 400 K and its latitudinal structure, sometimes termed the "horizontal tape-recorder" (e.g., Randel et al., 2001; Flury et al., 2013). Consistent with the discussion above, a transport barrier at the equator has only a very weak effect, weakly drying the SH subtropics and mid-latitudes, indicating only a minor role of the NH in moistening the SH lowest stratosphere. Furthermore, the effect of horizontal transport on the SH is small in all simulation, as H_2O mixing ratios in the SH are strongly affected by local freeze-drying at SH high-latitudes. In the NH, horizontal transport moistens the extratropical lower stratosphere in summer, and dries this region in winter. In the tropics, the annual cycle is related to minimum tropopause temperatures during boreal winter and maximum tropopause temperatures during summer. Therefore, during winter, horizontal transport exports dry air out of the tropics into the NH, and, during summer, moist air. Consequently, the entire annual cycle of LS H_2O in the NH extratropics is related to horizontal transport out of the subtropics, as argued by Ploeger et al. (2013). The boreal summer maxima are related to monsoonal circulations and transport out of the tropics, along the eastern and western flanks (Randel and Jensen, 2013).

Atmos. Chem. Phys. Discuss., https://doi.org/10.5194/acp-2017-1072
Manuscript under review for journal Atmos. Chem. Phys.
Discussion started: 30 November 2017

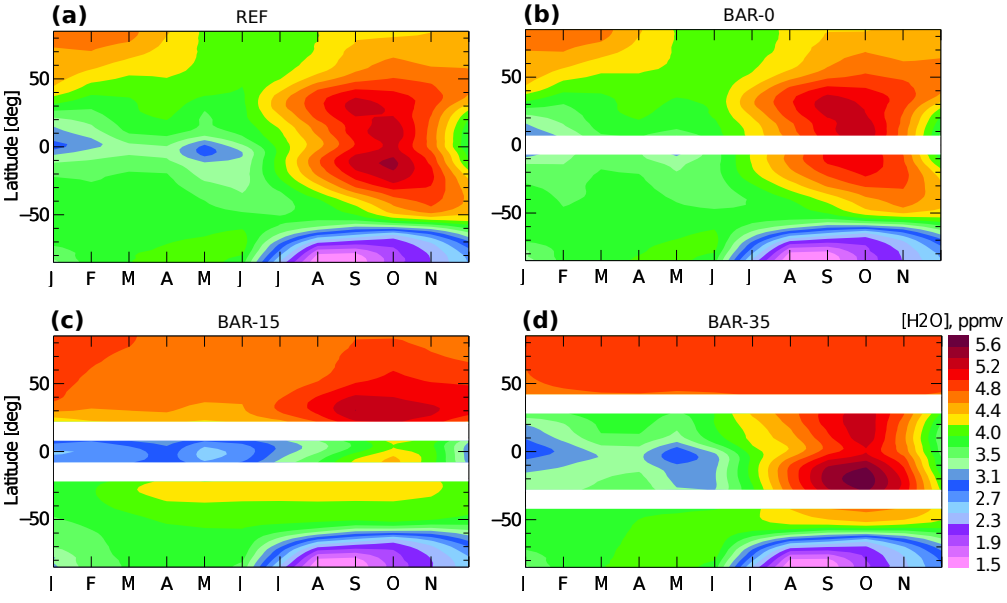

Figure 9. Horizontal tape-recorder of water vapour at the potential temperature level θ = 400 K for 2011. Shown data are from CLaMS sensitivity simulations for the reference (a) and the sensitivity simulations with transport barriers along latitude circles at 0° (b), 15° N/S (c) and 35° N/S (d). Transport barriers are represented in white.

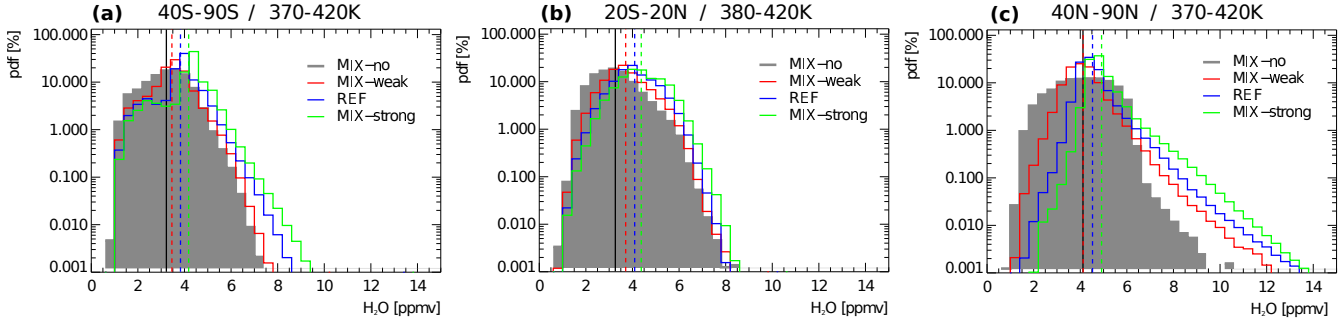

Figure 10. Probability density function (PDF) for water vapour mixing ratios in the SH extratropics for 40°S-90°S between 370 K and 420 K (a), in the tropics for 20°S-20°N between 380 K and 420 K (b), and in the NH extratropics for 40°N-90°N between 370 K and 420 K (c). Shown data are from 2011 CLaMS sensitivity simulations with different strength of small-scale mixing for the case without mixing (MIX-no, grey shading background), weak mixing (MIX-weak, red solid line), reference simulation (REF, blue solid line) and strong mixing (MIX-strong, green solid line). Dashed coloured lines represent the mean H_2O values for the different simulations respectively, whereas the black solid line shows the mean value for the non-mixing case.

Atmos. Chem. Phys. Discuss., https://doi.org/10.5194/acp-2017-1072
Manuscript under review for journal Atmos. Chem. Phys.
Discussion started: 30 November 2017

Atmospheric Chemistry and Physics Discussions

3.3 Mixing effects

The PDF of H_2O mixing ratio in Figure 10 shows that increased small-scale mixing in the model generally moistens the LS in the tropics, as well as in the extratropics of both hemispheres. Increased mixing causes both a decrease in the fraction of dry air and an increase in the fraction of moist air, and therefore shifts the PDF to higher mixing ratios. In particular, for the NH extratropics, this effect is strong, substantially enhancing the tail of the PDF at high mixing ratios. Therefore, the high mixing ratios are absent in the simulation without mixing. The mean H_2O mixing ratio is also increasing towards higher values with increasing mixing strength (dashed lines in Fig. 10).

Changes in the parametrized small-scale mixing strength, however, may affect different processes, critical to the distribution of H_2O in the LS region. Such processes are: diffusive cross-tropopause moisture transport, recirculation of air masses, permeability of the tropical pipe, and vertical diffusion (for illustration see Fig. 11). Therefore, interpreting the mixing effects in terms of processes is a challenging task.

Figure 12 shows annual zonal mean distributions of H_2O (a-d), total water (e-h). Similarly, Figure 13 shows double methane mixing ratios (a-d) and AoA (e-h) from the CLaMS simulation without mixing (MIX-no) and their incremental differences

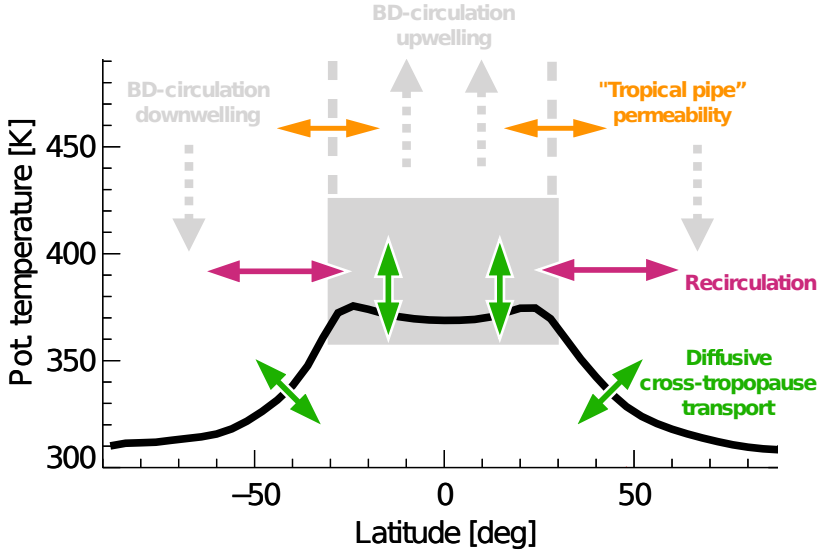

Figure 11. A schematic of considered processes critical for the distribution of water vapour in the LS region. Grey arrows represent Brewer-Dobson upwelling throughout the tropical region and downwelling towards the poles; green arrows stand for cross-tropopause transport through the whole latitudinal range; the pink arrows represent the region of recirculation of air masses in TTL and the orange arrows show the regions of "tropical pipe“ permeability. TTL is represented with solid grey background.

Atmos. Chem. Phys. Discuss., https://doi.org/10.5194/acp-2017-1072
Manuscript under review for journal Atmos. Chem. Phys.
Discussion started: 30 November 2017

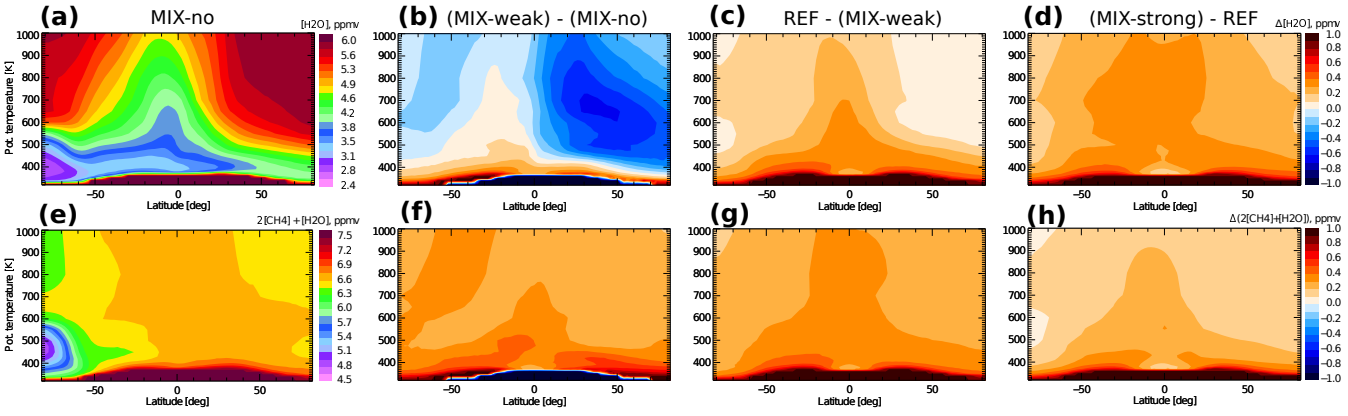

Figure 12. Annual zonal mean distributions of water vapour (a) and total water (e) from the CLaMS simulation without mixing (MIX-no), as well as the incremental differences between the sensitivity simulations with increasing mixing from the weak mixing case (MIX-weak) through the reference (REF) to the strong mixing case (MIX-strong); i.e. [(MIX-weak) - MIX-no] in the second column (b, f), [REF - (MIX-weak)] in the third column (c, g), and [(MIX-strong) - REF] in the fourth column (d, h).

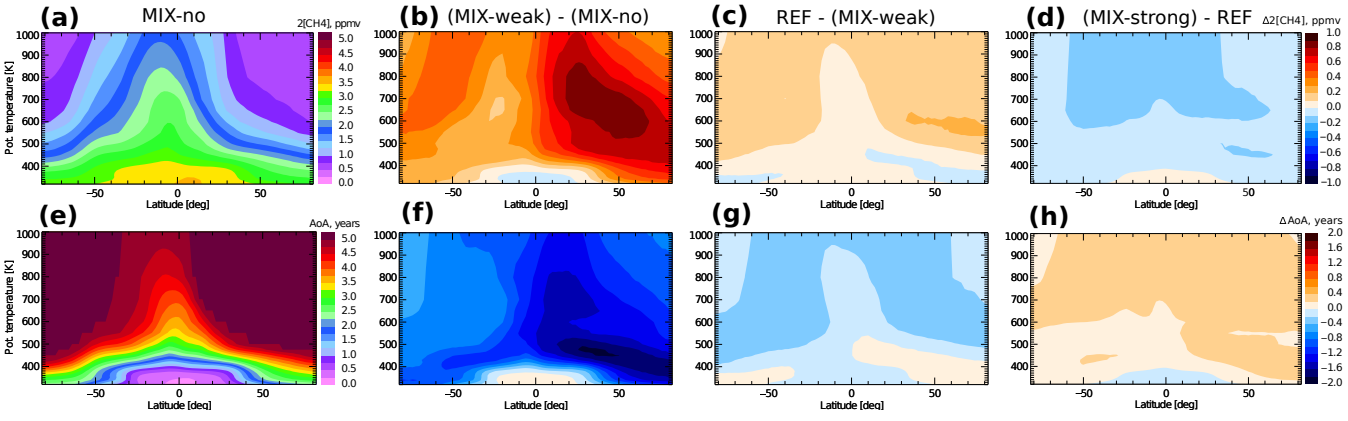

Figure 13. Annual zonal mean distributions of $2CH_4$ (a) and mean age of air (b) from the CLaMS simulation without mixing (MIX-no), as well as the incremental differences between the sensitivity simulations with increasing mixing from the weak mixing case (MIX-weak) through the reference (REF) to the strong mixing case (MIX-strong); i.e. [(MIX-weak) - MIX-no] in the second column (b, f), [REF - (MIX-weak)] in the third column (c, g), and [(MIX-strong) - REF] in the fourth column (d, h).

between the sensitivity simulations with increasing mixing from the weak mixing case (MIX-weak) through the reference (REF) to the strong mixing case (MIX-strong); i.e. [(MIX-weak) - MIX-no], [REF - (MIX-weak)], and [(MIX-strong) - REF]. Note that the simulation without small-scale mixing (MIX-no) should not be considered as a realistic case, as turbulent mixing processes always take place in the atmosphere. However, we show the results from this simulation for the sake of completeness,

Atmos. Chem. Phys. Discuss., https://doi.org/10.5194/acp-2017-1072
Manuscript under review for journal Atmos. Chem. Phys.
Discussion started: 30 November 2017

Atmospheric Chemistry and Physics Discussions

when analysing the mixing effects, and for facilitating comparisons with pure trajectory studies (e.g., Fueglistaler and Haynes, 2005; Schoeberl and Dessler, 2011).

A clear response to mixing is found for the lower stratosphere below ≈ 430 K, which is moistened with increasing small-scale mixing. In the following, we consider total water above the tropical tropopause as an indicator of changes in transport because it is not affected by chemistry (here methane oxidation). As the moistening below 430 K is also evident in total water, but not in methane and mean age, it is largely related to enhanced diffusive cross-tropopause transport of moist air. This enhanced diffusive cross-tropopause transport in turn increases the probability to by-pass the regions of cold temperatures, rendering the freeze-drying at the tropical tropopause less efficient. Consequently, H_2O entering the stratosphere is enhanced with increased small-scale mixing. The response of total water to changes in mixing is largely independent on the reference mixing strength throughout the stratosphere, with total water always increasing with increasing mixing (Fig. 12f, g, h), reflecting the fact that the efficiency of freeze-drying at the tropical tropopause decreases with increasing mixing.

Above about 430 K, the response of H_2O mixing ratio to varying the mixing strength turns out to be more challenging to interpret, and strongly depends on the reference strength of mixing, due to a complex interplay between horizontal and vertical mixing processes. First, increasing the mixing strength from no-mixing (MIX-no) to weak mixing (MIX-weak) causes significant drying in the NH (Fig. 12b). An analogous signal is evident in methane (Fig. 13b) and mean age (Fig. 13f), but not in total water (Figure 12f). Hence, the drying response in the NH is attributable to transport effects, most likely to an increased

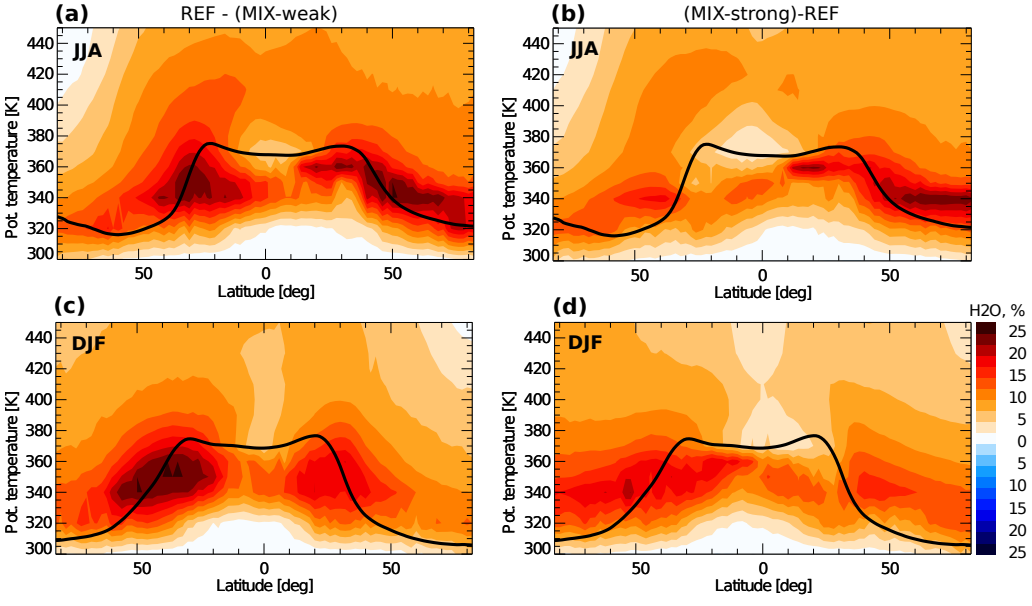

Figure 14. Differences of zonal mean water vapour for summer (a, b) and winter (c, d) seasons for 2011 between the reference and weak mixing and between the strong mixing and reference case for the LS region. Tropopause is presented with black solid line, and is calculated from ERA-Interim reanalysis data.

Atmos. Chem. Phys. Discuss., https://doi.org/10.5194/acp-2017-1072
Manuscript under review for journal Atmos. Chem. Phys.
Discussion started: 30 November 2017

Atmospheric Chemistry and Physics Discussions

permeability of the tropical pipe with increasing mixing and related increased transport of dry air and enhanced methane out of the tropics and into the NH. Second, increasing the mixing strength from weak mixing (MIX-weak) to reference mixing (REF) and from reference mixing to strong mixing (MIX-strong) causes a moister stratosphere globally, related to enhanced diffusive cross-tropopause transport, and less efficient freeze-drying (see discussion above). For the former (increasing mixing from MIX-weak), a weak increase of methane in the NH (Fig. 13c) indicates a simultaneous increase in the permeability of the tropical pipe. For the latter (increasing mixing from REF), decreasing methane mixing ratios (Fig. 13d) and increasing mean age (Fig. 13h) throughout the stratosphere, likely indicate a simultaneous increase in the strength of recirculation, due to increasing mixing.

Figure 14 presents a zoom-in view onto the H_2O response to mixing changes in the UTLS region, a critical region for global climate, for both summer (a, b) and winter (c, d). Clearly, enhanced small-scale mixing moistens the LS, due to enhanced diffusive cross-tropopause moisture transport, with maximum differences between the simulations of around 20%. The moistening effects are particularly large in the region around the tropopause, where the radiative effect is most sensitive (e.g., Riese et al., 2012). Furthermore, the moistening effect due to mixing maximizes in the summer hemisphere (Konopka et al., 2007). In the SH, H_2O in the subtropical jet regions appears to be most critical to changes in small-scale mixing. In particular, increasing H_2O mixing ratios in the extratropical lowermost stratosphere cause a flattening of the H_2O isopleths towards high latitudes.

Maps of the H_2O distribution at 400 K for the different CLaMS simulations with different small-scale mixing strength show the regions most prone to mixing changes (Fig. 15). Strongest moistening, due to increased mixing, occurs in the regions of

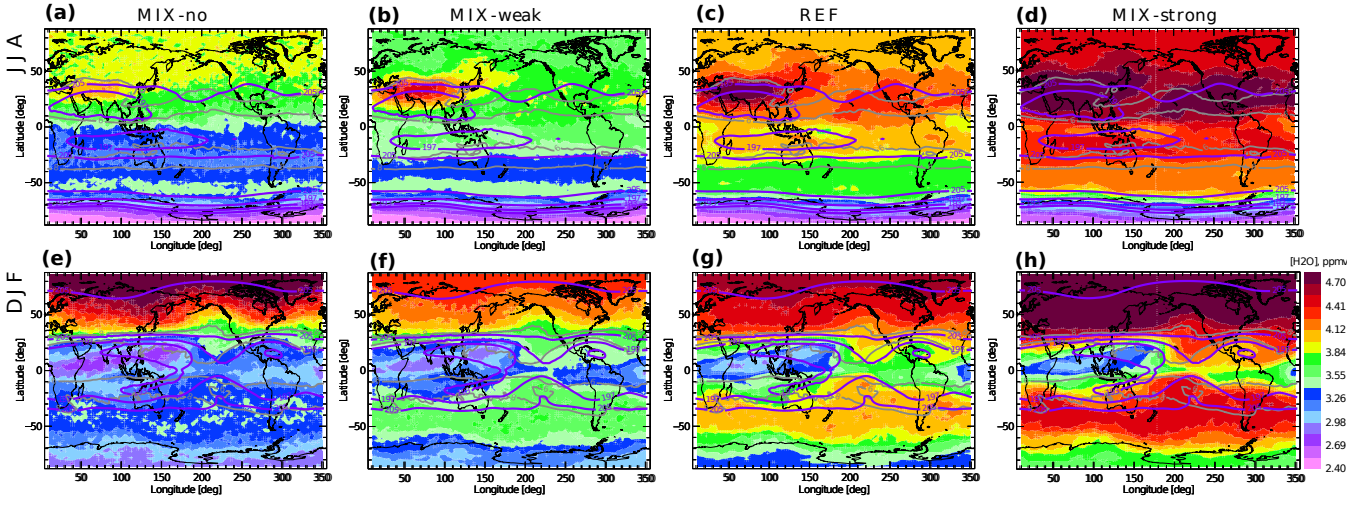

Figure 15. Seasonal mean water vapour distribution for 2011 from the CLaMS simulation without mixing (MIX-no) and the sensitivity simulations with non-vanishing mixing strength (MIX-weak, REF, MIX-strong) at the potential temperature level of 400 K; DJF indicates winter (a-d), and JJA summer periods (e-h). Grey lines are potential vorticity from ERA-Interim reanalysis data (6 PVU, 8 PVU), and the violet ones are temperatures (191 K, 193 K, 197 K, 205 K) taken from ERA-Interim reanalysis data

subtropical jets. This is consistent with the findings of Konopka and Pan (2012), showing that the subtropical jets are regions of intense mixing. Furthermore, the moist anomaly of the Asian monsoon during boreal summer is affected by small-scale mixing. Without mixing only a weak anomaly occurs. With increased mixing this anomaly first increases. When mixing becomes very strong (MIX-strong) the monsoon anomaly weakens again and the entire jet region becomes strongly moistened.

4 Discussion

The comparison between the reanalysis own specific humidity products and H_2O simulated with CLaMS driven by the meteorology of the same reanalysis reveals further insights into the control processes of H_2O in the reanalysis. Figure 16 shows H_2O mixing ratios in the LS at 380 K for winter and summer, as provided by ERA-Interim and JRA-55 specific humidity variables. Although the two CLaMS simulations driven by either ERA-Interim or JRA-55 showed differences in the details of the patterns (Fig. 5), both simulations agreed reliable well with the satellite observations. The reanalysis H_2O products, on the other hand, show a very different pattern (Fig. 16). Despite their success in describing the main dehydration regions in the deep tropics (mainly in the West Pacific, and over South America in boreal winter), they fail in representing the main moisture sources in the Asian and American monsoons during summer. ERA-Interim, for instance, shows highest summertime H_2O mixing ratios above the Pacific.

The clearest difference to MLS and CLaMS, however, occurs for JRA-55 H_2O in the middle and high latitude LS. In this region, JRA-55 H_2O mixing ratios are about one order of magnitude higher than ERA-Interim. A similar result was recently noticed by Davis et al. (2017), where they showed that JRA-55 strongly overestimates the amplitude of the seasonal H_2O cycle, although this result depends on the considered level. On the contrary, using the reanalysis temperature and wind fields to drive CLaMS transport and calculate stratospheric H_2O from the CLaMS cirrus dehydration scheme based on the Clausius-Clapeyron relation and simplified fall-out of ice particles (see Sect. 2), results in H_2O distributions in agreement with MLS observations. The different CLaMS simulations also show a moister stratosphere for JRA-55, compared to ERA-Interim, consistent with a warmer tropical tropopause in JRA-55, but with much smaller differences than for the reanalysis H_2O products. Although both reanalysis assimilation systems are constrained with observational data to produce realistic temperatures, significant differences around the tropical tropopause still exist of about 2 K (see Sect. 3.1). But these differences are not sufficient to explain the water vapour differences between the reanalysis products, as presented in Figure 16. Hence, the reanalysis own H_2O products seem not consistent with the simple Clausius-Clapeyron relation.

Figure 17 shows H_2O PDFs for further insights into the processes causing the difference between ERA-Interim and JRA-55 H_2O in the extratropical LS. Both CLaMS simulations, driven with either ERA-Interim or JRA-55 data, and ERA-Interim reanalysis H_2O products show a skewed PDF with a tail at high values, particularly strong in boreal summer. JRA-55 H_2O mixing ratios, on the contrary, show a PDF with a totally different shape and a much higher mean value by about a factor of 5. The different shape of the JRA-55 PDFs, with the peak at much higher mixing ratios, suggests that high H_2O mixing ratios are deposited in the extratropical LS, up to potential temperature levels of about 380 K, potentially related to the convective scheme in the reanalysis. JRA-55 shows a higher frequency of high and optically thick clouds, when compared with ERA-Interim (e.g.,

Atmos. Chem. Phys. Discuss., https://doi.org/10.5194/acp-2017-1072
Manuscript under review for journal Atmos. Chem. Phys.
Discussion started: 30 November 2017

Atmospheric Chemistry and Physics Discussions

Kang and Ahn, 2015; Kobayashi et al., 2015; Tompkins et al., 2007), which also could hint at a critical role of differences in convection for causing the differences in H_2O (e.g., Folkins and Martin, 2005; Sherwood et al., 2010).

5 Conclusions

We investigated the sensitivities of modelling H_2O in the LS region regarding different reanalysis datasets, horizontal transport between tropics and extratropics, and small-scale mixing, using the Lagrangian transport model CLaMS.

Differences in H_2O between model simulations driven by ERA-Interim and JRA-55 reanalysis amount to about 0.5 ppmv throughout the stratosphere. This demonstrates a substantial uncertainty in simulated H_2O, even when using the most recent reanalysis products. This uncertainty in simulated H_2O results mainly from differences in temperatures between the reanalysis products around the tropical tropopause, indicating that tropopause temperatures in the reanalysis are not sufficiently constrained.

Through sensitivity simulations, where we have introduced artificial transport barriers in the model to suppress certain horizontal transport pathways, we find that the overall effects of interhemispheric transport is weak and insignificant for strato-

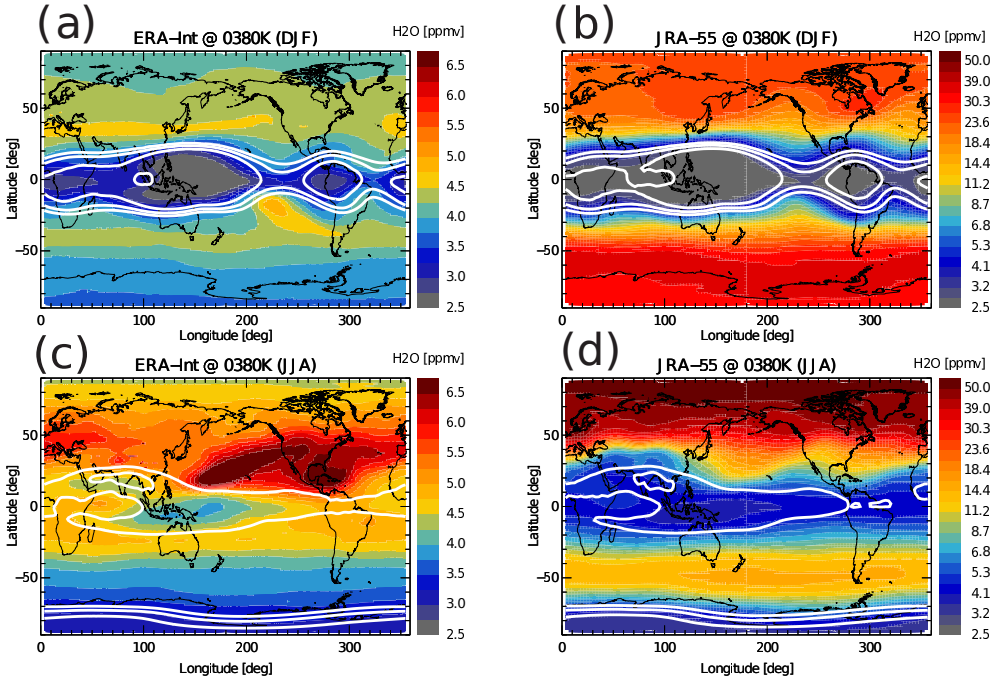

Figure 16. Seasonal mean water vapour distribution averaged over the period from 2004 to 2013 at the potential temperature level of 380 K; DJF indicates winter (a, b), and JJA summer periods (c, d). Shown data are from both reanalysis, ERA-Interim and JRA-55 reanalysis data. The white lines are constant temperature levels from corresponding reanalysis datasets (191 K, 193 K, 195 K). Note the logarithmic colorbar for JRA-55.

Atmos. Chem. Phys. Discuss., https://doi.org/10.5194/acp-2017-1072
Manuscript under review for journal Atmos. Chem. Phys.
Discussion started: 30 November 2017

spheric H_2O. Furthermore, our results suggest that the NH subtropics are a critical source region of moisture for the global stratosphere, likely related to the subtropical monsoon circulations. Hence, a reliable representation of processes in the subtropics in global models turns out to be critical for simulating stratospheric H_2O and its climate effects.

Changing the strength of small-scale mixing in CLaMS shows that increased mixing causes moistening of the stratosphere, by enhanced diffusive moisture transport across the tropopause. The strongest mixing effects occur around the subtropical jets. Above about 430 K, increased mixing causes a complex interplay between vertical and horizontal mixing, which results in both moistening or drying of the stratosphere depending on the mixing strength. Therefore, interpretation of differences in simulated water vapour from different models in terms of differences in numerical diffusion is a challenging task. The results from our sensitivity simulations are aimed to guide the interpretation of model differences and to pinpoint model deficits.

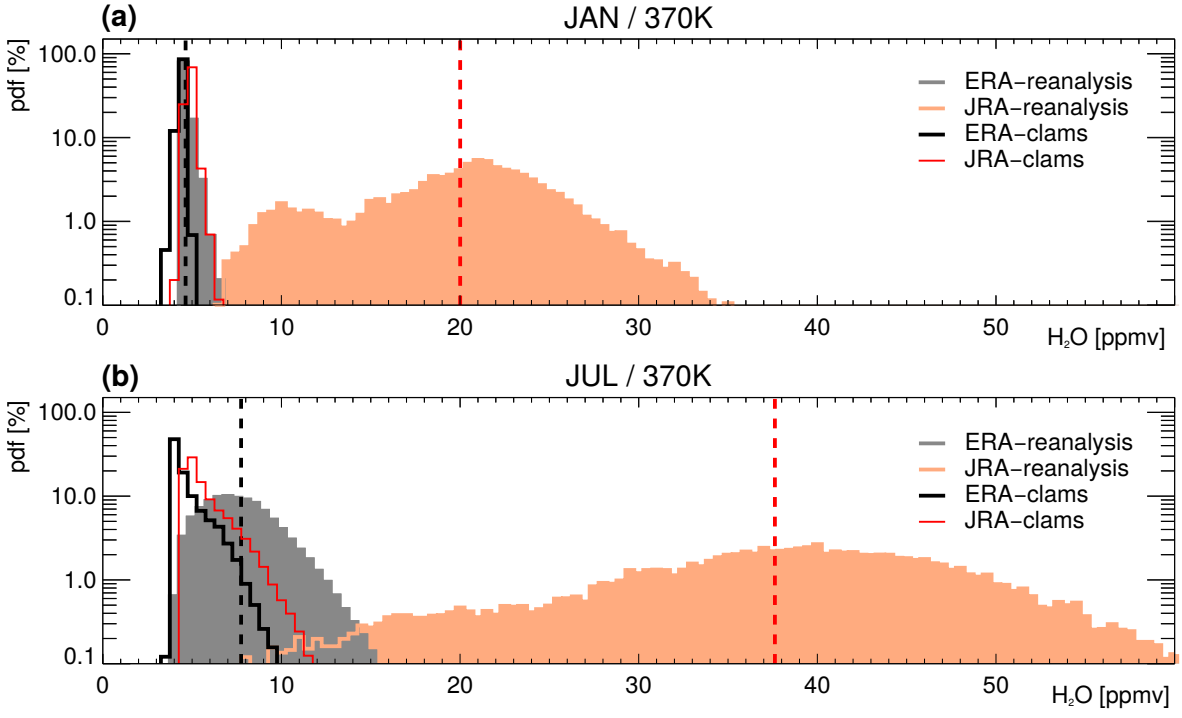

Figure 17. Probability density function (PDF) for water vapour mixing ratio for 2011, at the potential temperature level of 370 K. The distribution is presented for January (a) and July (b). Shown data are taken from ERA-Interim (grey line) and JRA-55 (orange line) reanalysis data. CLaMS water vapour driven by ERA-Interim (black line) and JRA-55 (red line) is shown for comparison. Vertical dashed lines are the mean values of the reanalysis data respectively, black one of ERA-Interim, red one is JRA-55 reanalysis products.

Atmos. Chem. Phys. Discuss., https://doi.org/10.5194/acp-2017-1072
Manuscript under review for journal Atmos. Chem. Phys.
Discussion started: 30 November 2017

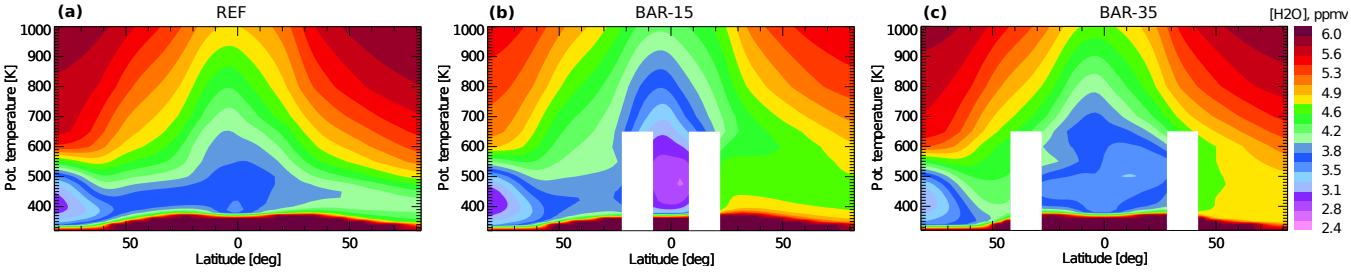

Figure A1. Zonal mean water vapour distribution averaged over the period from 2011 to 2014. Shown data are from CLaMS sensitivity simulations for the reference (a) and the horizontal transport barrier simulations with barriers along 15° N/S (b) and 35° N/S (c). Barriers are set between the Earth's surface and the 600 K potential temperature levels and are represented in white.

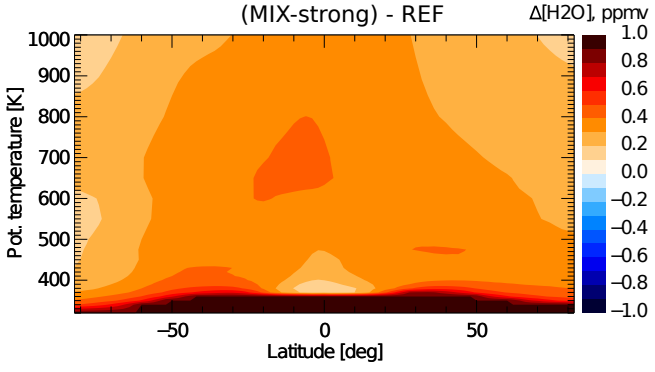

Figure A2. Differences of zonal mean water vapour from CLaMS sensitivity simulations with non-vanishing mixing strength between reference (REF) and strong mixing (MIX-strong) cases averaged over the period from 2011 to 2014.

Appendix A: Validation of the simulations

In order to study the robustness of our conclusions concerning changes in the simulation period, we carried out some of the simulations for the entire period between 2011 and 2014. Figure A1 shows the distribution of zonal mean H_2O mixing ratios for this period for the reference (a) and horizontal barrier simulations with barriers at 15°N/S (b) and 35°N/S (c). Clearly, the differences between the different simulations with transport barriers stay qualitatively similar, when compared to the 2011 case (see Fig. 8). Although, the results for the year 2011 appear slightly drier when compared to 2011-2014, likely related to the occurrence of La Niña in 2011.

Also the effects of increased small-scale mixing for 2011 are consistent with the climatological data for the 2011-2014 period (Fig. A2). Although the effect of increasing the mixing strength appears even stronger for 2011-2014. As a conclusion, restricting our analysis to a single year has no significant effect on our conclusions, which can be regarded as representative for the climatological case.

Acknowledgements. We thank Jens-Uwe Grooß for the helpful discussion. Also we are very appreciative of the ECMWF for providing reanalysis data, the MLS and ACE-FTS teams for providing satellite observation data. The Atmospheric Chemistry Experiment (ACE), also known as SCISAT, is a Canadian-led mission mainly supported by the Canadian Space Agency and the Natural Sciences and Engineering Research Council of Canada. In addition, we gratefully acknowledge the computing time granted on the supercomputer JURECA at Jülich Supercomputing Centre (JSC) under the VSR project ID JICG11. This work was partly funded by the German Ministry of Education and Research under grant no. 01LG1222A (ROMIC-TRIP), and partly by the Helmholtz Young Investigators Group A-SPECi ("Assessment of stratospheric processes and their effects on climate variability").

References

Avery, M. A., Davis, S. M., Rosenlof, K. H., Ye, H., and Dessler, A. E.: Large anomalies in lower stratospheric water vapour and ice during the 2015–2016 El Niño, NATURE GEOSCIENCE, 10, 405–410, https://doi.org/10.1038/NGEO2961, 2017.

Bannister, R. N., O'Neill, A., Gregory, A. R., and Nissen, K. M.: The role of the south-east Asian monsoon and other seasonal features in creating the 'tape-recorder' signal in the Unified Model, Q. J. R. Meteorol. Soc., 130, 1531–1554, 2004.

Bernath, P.: The Atmospheric Chemistry Experiment (ACE), J. Quant. Spectr. Radiat. Transfer, 186, 3–16, https://doi.org/10.1016/j.jqsrt.2016.04.006, 2017.

Bernath, P. F., McElroy, C. T., Abrams, M. C., Boone, C. D., Butler, M., Camy-Peyret, C., Carleer, M., Clerbaux, C., Coheur, P.-F., Colin, R., DeCola, P., DeMazière, M., Drummond, J. R., Dufour, D., Evans, W. F. J., Fast, H., Fussen, D., Gilbert, K., Jennings, D. E., Llewellyn, E. J., Lowe, R. P., Mahieu, E., McConnell, J. C., McHugh, M., McLeod, S. D., Michaud, R., Midwinter, C., Nassar, R., Nichitiu, F., Nowlan, C., Rinsland, C. P., Rochon, Y. J., Rowlands, N., Semeniuk, K., Simon, P., Skelton, R., Sloan, J. J., Soucy, M.-A., Strong, K., Tremblay, P., Turnbull, D., Walker, K. A., Walkty, I., Wardle, D. A., Wehrle, V., Zander, R., and Zou, J.: Atmospheric Chemistry Experiment (ACE) Mission overview, Geophys. Res. Lett., 32, L15S01, https://doi.org/10.1029/2005GL022386, 2005.

Brewer, A. W.: Evidence for a world circulation provided by the measurements of helium and water vapour distribution in the stratosphere, Q. J. R. Meteorol. Soc., 75, 351–363, https://doi.org/10.1002/qj.49707532603, 1949.

Davis, S. M., Hegglin, M. I., Fujiwara, M., Dragani, R., Harada, Y., Kobayashi, C., Long, C., Manney, G. L., Nash, E. R., Potter, G. L., Tegtmeier, S., Wang, T., Wargan, K., and Wright, J. S.: Assessment of upper tropospheric and stratospheric water vapor and ozone in reanalyses as part of S-RIP, Atmos. Chem. Phys., 17, 12 743–12 778, https://doi.org/10.5194/acp-17-12743-2017, 2017.

Dee, D. P., Uppala, S. M., Simmons, A. J., Berrisford, P., Poli, P., Kobayashi, S., Andrae, U., Balmaseda, M. A., Balsamo, G., Bauer, P., Bechtold, P., Beljaars, A. C. M., van de Berg, L., Bidlot, J., Bormann, N., Delsol, C., Dragani, R., Fuentes, M., Geer, A. J., Haimberger, L., Healy, S. B., Hersbach, H., Holm, E. V., Isaksen, L., Kallberg, P., Koehler, M., Matricardi, M., McNally, A. P., Monge-Sanz, B. M., Morcrette, J.-J., Park, B.-K., Peubey, C., de Rosnay, P., Tavolato, C., Thepaut, J.-N., and Vitart, F.: The ERA-Interim reanalysis: configuration and performance of the data assimilation system, Q. J. R. Meteorol. Soc., 137, 553–597, https://doi.org/10.1002/qj.828, 2011.

Dessler, A., Schoeberl, M., Wang, T., Davis, S., and Rosenlof, K.: Stratospheric water vapor feedback, Proceedings of the National Academy of Sciences, 110, 18 087–18 091, https://doi.org/10.1073/pnas.1310344110, 2013.

Dessler, A. E., Weinstock, E. M., Hintsa, E. J., Anderson, J. G., Webster, C. R., May, R. D., Elkins, J. W., and Dutton, G. S.: An examination of the total hydrogen budget of the lower stratosphere, Geophys. Res. Lett., 21, 2563–2566, https://doi.org/10.1029/94GL02283, 1994.

Flury, T., Wu, D. L., and Read, W. G.: Variability in the speed of the Brewer-Dobson circulation as observed by Aura/MLS, Atmos. Chem. Phys., 13, 4563–4575, https://doi.org/10.5194/acp-13-4563-2013, 2013.

Folkins, I. and Martin, R. V.: The vertical structure of tropical convection and its impact on the budget of water vapor and ozone, J. Atmos. Chem., 62, 1560–1573, 2005.

Forster, P. and Shine, K. P.: Stratospheric water vapour change as possible contributor to observed stratospheric cooling, Geophys. Res. Lett., 26, 3309 – 3312, https://doi.org/10.1029/1999GL010487, 1999.

Forster, P. and Shine, K. P.: Assessing the climate impact of trends in stratospheric water vapor, Geophys. Res. Lett., 29, 1086, https://doi.org/10.1029/2001GL013909, http://dx.doi.org/10.1029/2001GL013909, 2002.

Fueglistaler, S. and Haynes, P. H.: Control of interannual and longer-term variability of stratospheric water vapor, J. Geophys. Res., 110, D24108, https://doi.org/10.1029/2005JD006019, 2005.

Fueglistaler, S., Dessler, A. E., Dunkerton, T. J., Folkins, I., Fu, Q., and Mote, P. W.: Tropical tropopause layer, Rev. Geophys., 47, RG1004, https://doi.org/10.1029/2008RG000267, 2009.

Gettelman, A., Hegglin, M. I., Son, S.-W., Birner, J. K. M. F. T., Kremser, S., Rex, M., Añel, J. A., Akiyoshi, H., Austin, J., Bekki, S., Braesicke, P., Brühl, C., Butchart, N., Chipperfield, M., Dameris, M., Dhomse, S., Garny, H., Hardiman, S., Jöckel, P., Kinnison, D., Lamarque, J. F., Mancini, E., Marchand, M., Michou, M., Morgenstern, O., Pawson, S., Pitari, G., Plummer, D. A., Pyle, J., Rozanov, E., Scinocca, J., Shepherd, T. G., Shibata, K., Smale, D., Teyssedre, H., , and Tian, W.: Multi-model Assessment of the Upper Troposphere and Lower Stratosphere: Tropics and Global Trends, J. Geophys. Res., 115, D00M08, https://doi.org/10.1029/2009JD013638, 2010.

Glanville, A. A. and Birner, T.: Role of vertical and horizontal mixing in the tape recorder signal near the tropical tropopause, Atmos. Chem. Phys., 17, 4337–4353, https://doi.org/10.5194/acp-17-4337-2017, 2017.

Hardiman, S. C., Boutle, I. A., Bushell, A. C., Butchart, N., Cullen, M. J. P., Field, P. R., Furtado, K., Manners, J. C., Milton, S. F., Morcrette, C., O'Connor, F. m., Shipway, B. J., Smith, C., Walters, D. N., Willett, M. R., Williams, K. D., Wood, N., Abraham, N. L., Keeble, J., Maycock, A. C., Thuburn, J., and Woodhouse, M. T.: Processes Controlling Tropical Tropopause Temperature and Stratospheric Water Vapor in Climate Models, JOURNAL OF CLIMATE, 28, https://doi.org/10.1175/JCLI-D-15-0075.1, 2015.

Haynes, P. and Anglade, J.: The vertical scale cascade in atmospheric tracers due to large-scale differential advection, J. Atmos. Sci., 54, 1121–1136, 1997.

Hegglin, M. I., Boone, C. D., Manney, G. L., Shepherd, T. G., Walker, K. A., Bernath, P. F., Daffer, W. H., Hoor, P., and Schiller, C.: Validation of ACE-FTS satellite data in the upper troposphere/lower stratosphere (UTLS) using non-coincident measurements, Atmos. Chem. Phys., 8, 1483–1499, 2008.

Hegglin, M. I., Plummer, D. A., Shepherd, T. G., Scinocca, J. F., Anderson, J., Froidevaux, L., Funke, B., Hurst, D., Rozanov, A., Urban, J., von Clarmann, T., A.Walker, K., Wang, H. J., Tegtmeier, S., and Weigel, K.: Vertical structure of stratospheric water vapour trends derived from merged satellite data, Nature Geoscience, 7, 768–776, https://doi.org/10.1038/NGEO2236, 2014.

Holton, J. R. and Gettelman, A.: Horizontal transport and the dehydration of the stratosphere, Geophys. Res. Lett., 28, 2799–2802, 2001.

Hurst, D. F., Read, W. G., Vömel, H., Selkirk, H. B., Rosenlof, K. H., Davis, S. M., Hall, E. G., Jordan, A. F., and Oltmans, S. J.: Recent divergences in stratospheric water vapor measurements by frost point hygrometers and the Aura Microwave Limb Sounder, Atmos. Meas. Tech., 9, 4447–4457, https://doi.org/10.5194/amt-9-4447-2016, 2016.

James, R., Bonazzola, M., Legras, B., Surbled, K., and Fueglistaler, S.: Water vapor transport and dehydration above convective outflow during Asian monsoon, Geophys. Res. Lett., 35, L20810, https://doi.org/10.1029/2008GL035441, 2008.

Kämpfer, N., ed.: Monitoring Atmospheric Water Vapour: Ground-Based Remote Sensing and In-situ Methods, Springer-Verlag New York, Bern, Switzerland, 2013.

Kang, S. and Ahn, J.-B.: Global Energy and Water Balances in the Latest Reanalyses, Asia-Pac. J. Atmos. Sci., 51, 293–302, https://doi.org/10.1007/s13143-015-0079-0, 2015.

Kobayashi, S., Ota, Y., Harada, Y., Ebita, A., Moriya, M., Onoda, H., Onogi, K., Kamahori, H., Kobayashi, C., a. E. H., Miyaoka, K., and Takahashi, K.: The JRA-55 Reanalysis: General Specifications and Basic Characteristics, Meteor. Soc. Japan, 93, 5–48, https://doi.org/10.2151/jmsj.2015-001, 2015.

Konopka, P. and Pan, L. L.: On the mixing-driven formation of the Extratropical Transition Layer (ExTL), J. Geophys. Res., 117, D18301, https://doi.org/10.1029/2012JD017876, 2012.

Konopka, P., Steinhorst, H.-M., Grooß, J.-U., Günther, G., Müller, R., Elkins, J. W., Jost, H.-J., Richard, E., Schmidt, U., Toon, G., and McKenna, D. S.: Mixing and Ozone Loss in the 1999-2000 Arctic Vortex: Simulations with the 3-dimensional Chemical Lagrangian Model of the Stratosphere (CLaMS), J. Geophys. Res., 109, D02315, https://doi.org/10.1029/2003JD003792, 2004.

Konopka, P., Günther, G., McKenna, D. S., Müller, R., Offermann, D., Spang, R., and Riese, M.: How homogeneous and isotropic is stratospheric mixing? Comparison of CRISTA-1 observations with transport studies based on the Chemical Lagrangian Model of the Stratosphere (CLaMS), Q. J. R. Meteorol. Soc., 131, 565–579, https://doi.org/10.1256/qj.04.47, 2005.

Konopka, P., Günther, G., Müller, R., dos Santos, F. H. S., Schiller, C., Ravegnani, F., Ulanovsky, A., Schlager, H., Volk, C. M., Viciani, S., Pan, L. L., McKenna, D.-S., and Riese, M.: Contribution of mixing to upward transport across the tropical tropopause layer (TTL), Atmos. Chem. Phys., 7, 3285–3308, 2007.

Konopka, P., Ploeger, F., and Müller, R.: Entropy- and static stability-based Lagrangian model grids, in: Geophysical Monograph Series: Lagrangian Modeling of the Atmosphere, edited by Lin, J., vol. 200, pp. 99–109, American Geophysical Union, https://doi.org/10.1029/2012GM001253, 2012.

Kremser, S., Wohltmann, I., Rex, M., Langematz, U., Dameris, M., and Kunze, M.: Water vapour transport in the tropical tropopause region in coupled Chemistry-Climate Models and ERA-40 reanalysis data, Atmos. Chem. Phys., 9, 2679–2694, 2009.

LeTexier, H., Solomon, S., and Garcia, R. R.: The role of molecular hydrogen and methane oxidation in the water vapour budget of the stratosphere, Q. J. R. Meteorol. Soc., 114, 281 – 295, 1988.

Liu, S., Fueglistaler, S., and Haynes, P.: Advection–condensation paradigm for stratospheric water vapor, J. Geophys. Res., 115, D24307, https://doi.org/10.1029/2010JD014352, 2011.

Livesey, N. J., Read, W. G., Wagner, P. A., Froidevaux, L., Lambert, A., Manney, G. L., Valle, L. F. M., Pumphrey, H. C., Santee, M. L., Schwartz, M. J., Wang, S., Fuller, R. A., Jarnot, R. F., Knosp, B. W., and Martinez, E.: Earth Observing System, Aura Microwave Limb Sounder (MLS): Version 4.2x Level 2 data quality and description document, Technical report, Jet Propulsion Laboratory, D-33509, 2017.

Mahowald, N. M., Plumb, R. A., Rasch, P. J., del Corral, J., and Sassi, F.: Stratospheric transport in a three-dimensional isentropic coordinate model, J. Geophys. Res., 107, 4254, https://doi.org/10.1029/2001JD001313, 2002.

Marti, J. and Mauersberger, K.: A survey and new measurements of ice vapor pressure temperatures between 170 and 250 K, Geophys. Res. Lett., 20, 363–366, https://doi.org/10.1029/93GL00105, 1993.

Maycock, A. C., Joshi, M. M., Shine, K. P., and Scaife, A. A.: The Circulation Response to Idealized Changes in Stratospheric Water Vapor, American Meteorological Society, 26, 545–561, https://doi.org/10.1175/JCLI-D-12-00155.1, 2013.

McKenna, D. S., Konopka, P., Grooß, J.-U., Günther, G., Müller, R., Spang, R., Offermann, D., and Orsolini, Y.: A new Chemical Lagrangian Model of the Stratosphere (CLaMS): 1. Formulation of advection and mixing, J. Geophys. Res., 107, 4309, https://doi.org/10.1029/2000JD000114, 2002a.

McKenna, D. S., Grooß, J.-U., Günther, G., Konopka, P., Müller, R., Carver, G., and Sasano, Y.: A new Chemical Lagrangian Model of the Stratosphere (CLaMS): 2. Formulation of chemistry scheme and initialization, J. Geophys. Res., 107, 4256, https://doi.org/10.1029/2000JD000113, 2002b.

Mote, P. W., Rosenlof, K. H., Holton, J. R., Harwood, R. S., and Waters, J. W.: Seasonal variations of water vapor in the tropical lower stratosphere, Geophys. Res. Lett., 22, 1093–1096, https://doi.org/10.1029/95GL01234, 1995.

Mote, P. W., Rosenlof, K. H., McIntyre, M. E., Carr, E. S., Gille, J. G., Holton, J. R., Kinnersley, J. S., Pumphrey, H. C., Russell III, J. M., and Waters, J. W.: An atmospheric tape recorder: The imprint of tropical tropopause temperatures on stratospheric water vapor, J. Geophys. Res., 101, 3989–4006, 1996.

Mote, P. W., Dunkerton, T. J., McIntyre, M. E., Ray, E. A., Haynes, P. H., and Russell III, J. M.: Vertical velocity, vertical diffusion, and dilution by midlatitude air in the tropical lower stratosphere, J. Geophys. Res., 103, 8651 – 8666, 1998.

Neu, J. L. and Plumb, R. A.: Age of air in a "leaky pipe" model of stratospheric transport, J. Geophys. Res., 104, 243–255, https://doi.org/10.1029/1999JD900251, 1999.

Orsolini, Y. J., Manney, G. L., Angel, A., Ovarlez, J., Claud, C., and Coy, L.: Layering in stratospheric profiles of long-lived trace species: Balloon-borne observations and modeling, J. Geophys. Res., 103, 5815–5825, 1998.

Pan, L. L., Solomon, S., Randel, W., Lamarque, J.-F., Hess, P., Gille, J., Chiou, E.-W., and McCormick, M. P.: Hemispheric asymmetries and seasonal variations of the lowermost stratospheric water vapor and ozone derived from SAGE II data, J. Geophys. Res., 102, https://doi.org/10.1029/97JD02778, 1997.

Pierrehumbert, R. T. and Rocca, R.: Evidence for control of Atlantic subtropical humidity by large scale advection, Geophys. Res. Lett., 25, 4537–4540, https://doi.org/10.1029/1998GL900203, 1998.

Ploeger, F., Konopka, P., Günther, G., Grooß, J.-U., and Müller, R.: Impact of the vertical velocity scheme on modeling transport across the tropical tropopause layer, J. Geophys. Res., 115, D03301, https://doi.org/10.1029/2009JD012023, 2010.

Ploeger, F., Konopka, P., Müller, R., Fueglistaler, S., Schmidt, T., Manners, J. C., Grooß, J.-U., Günther, G., Forster, P. M., and Riese, M.: Horizontal transport affecting trace gas seasonality in the Tropical Tropopause Layer (TTL), J. Geophys. Res., 117, D09303, https://doi.org/10.1029/2011JD017267, 2012.

Ploeger, F., Günther, G., Konopka, P., Fueglistaler, S., Müller, R., Hoppe, C., Kunz, A., Spang, R., Grooß, J.-U., and Riese, M.: Horizontal water vapor transport in the lower stratosphere from subtropics to high latitudes during boreal summer, J. Geophys. Res., 118, 8111–8127, https://doi.org/10.1002/jgrd.50636, 2013.

Ploeger, F., Abalos, M., Birner, T., P.Konopka, Legras, B., Müller, R., and Riese, M.: Quantifying the effects of mixing and residual circulation on trends of stratospheric mean age of air, Geophys. Res. Lett., 42, 2047–2054, https://doi.org/10.1002/2014GL062927, 2015.

Pommrich, R., Müller, R., Grooß, J.-U., Konopka, P., Ploeger, F., Vogel, B., Tao, M., Hoppe, C. M., Günther, G., Spelten, N., Hoffmann, L., Pumphrey, H.-C., Viciani, S., D'Amato, F., Volk, C. M., Hoor, P., Schlager, H., and Riese, M.: Tropical troposphere to stratosphere transport of carbon monoxide and long-lived trace species in the Chemical Lagrangian Model of the Stratosphere (CLaMS), Geoscientific Model Development, 7, 2895–2916, https://doi.org/10.5194/gmd-7-2895-2014, http://www.geosci-model-dev.net/7/2895/2014/, 2014.

Randel, W. and Jensen, E.: Physical processes in the tropical tropopause layer and their role in a changing climate, Nature Geoscience, 6, 169–176, https://doi.org/10.1038/ngeo1733, 2013.

Randel, W. J., Wu, F., Russell, J. M., Roche, A., and Waters, J. W.: Seasonal cycles and QBO variations in stratospheric CH_4 and H_2O observed in UARS HALOE data, J. Atmos. Sci., 55, 163–185, 1998.

Randel, W. J., Wu, F., Gettelman, A., Russell, J., Zawodny, J., and Oltmans, S.: Seasonal variation of water vapor in the lower stratosphere observed in Halogen Occultation Experiment data, J. Geophys. Res., 106, D13, https://doi.org/10.1029/2001JD900048, 2001.

Riese, M., Ploeger, F., Rap, A., Vogel, B., Konopka, P., Dameris, M., and Forster, P.: Impact of uncertainties in atmospheric mixing on simulated UTLS composition and related radiative effects, J. Geophys. Res., 117, D16305, https://doi.org/10.1029/2012JD017751, 2012.

Rodgers, C. D.: Inverse methods for atmospheric sounding: theory and practice, vol. 2 of *Series on atmospheric, oceanic and planetary physics*, World Scientific, Singapore, 2000.

Rohs, S., Schiller, C., Riese, M., Engel, A., Schmidt, U., Wetter, T., Levin, I., Nakazawa, T., and Aoki, S.: Long-term changes of methane and hydrogen in the stratosphere in the period 1978 – 2003 and their impact on the abundance of stratospheric water vapor, J. Geophys. Res., 111, D14315, https://doi.org/10.1029/2005JD006877, 2006.

Rosenlof, K. H., Tuck, A. F., Kelly, K. K., Russell III, J. M., and McCormick, M. P.: Hemispheric asymmetries in the water vapor and inferences about transport in the lower stratosphere, J. Geophys. Res., 102, 13 213–13 234, https://doi.org/10.1029/97JD00873, 1997.

Schoeberl, M. R. and Dessler, A. E.: Dehydration of the stratosphere, Atmos. Chem. Phys., 11, 8433–8446, https://doi.org/10.5194/acp-11-8433-2011, 2011.

Schoeberl, M. R., Dessler, A. E., and Wang, T.: Modeling upper tropospheric and lower stratospheric water vapor anomalies, Atmos. Chem. Phys., 13, 7783–7793, https://doi.org/10.5194/acp-13-7783-2013, 2013.

Sherwood, S. C., Roca, R., Weckwerth, T. M., and Andronova, N. G.: Tropospheric water vapor, convection, and climate, Rev. Geophys., 48, RG2001, https://doi.org/10.1029/2009RG000301, 2010.

Solomon, S., Rosenlof, K., Portmann, R., Daniel, J., Davis, S., Sanford, T., and Plattner, G.-K.: Contributions of stratospheric water vapor to decadal changes in the rate of global warming, Science, 327, 1219–1223, https://doi.org/10.1126/science.1182488, 2010.

Stenke, A., Dameris, M., Grewe, V., and Garny, H.: Implications of Lagrangian transport for coupled chemistry-climate simulations, Atmos. Chem. Phys. Discuss., 8, 18 727–18 764, 2008.

Tompkins, A. M., Gierens, K., and Rädel, G.: Ice supersaturation in the ECMWF Integrated Forecast System., Q. J. R. Meteorol. Soc., 133, 53–63, https://doi.org/10.1002/qj.14, 2007.

Waters, J., Froidevaux, L., Jarnot, R., Read, W., Pickett, H., Harwood, R., Cofield, R., Filipiak, M., Flower, D., Livesey, N., Manney, G., Pumphrey, H., Santee, M., Siegel, P., and Wu, D.: Earth Observing System (EOS) Microwave Limb Sounder (MLS). An overview of the EOS MLS experiment, Technical report, Jet Propulsion Laboratory, D-15745, 2004.

Waters, J. W., Froidevaux, L., Harwood, R. S., Jarnot, R. F., Pickett, H. M., Read, W. G., Siegel, P. H., Cofield, R. E., Filipiak, M. J., Flower, D. A., Holden, J. R., Lau, G. K., Livesey, N. J., Manney, G. L., Pumphrey, H. C., Santee, M. L., Wu, D. L., Cuddy, D. T., Lay, R. R., Loo, M. S., Perun, V. S., Schwartz, M. J., Stek, P. C., Thurstans, R. P., Boyles, M. A., Chandra, K. M., Chavez, M. C., Chen, G.-S., Chudasama, B. V., Dodge, R., Fuller, R. A., Girard, M. A., Jiang, J. H., Jiang, Y., Knosp, B. W., LaBelle, R. C., Lam, J. C., Lee, K. A., Miller, D., Oswald, J. E., Patel, N. C., Pukala, D. M., Quintero, O., Scaff, D. M., Snyder, W. V., Tope, M. C., Wagner, P. A., and Walch, M. J.: The Earth Observing System Microwave Limb Sounder (EOS MLS) on the Aura Satellite, J. Atmos. Sci., 56, 194–217, https://doi.org/10.1175/1520-0469(1999)056, 1999.

Waters, J. W., Froidevaux, L., Harwood, R. S., Jarnot, R. F., Pickett, H. M., Read, W. G., Siegel, P. H., Cofield, R. E., Filipiak, M. J., Flower, D. A., Holden, J. R., Lau, G. K., Livesey, N. J., Manney, G. L., Pumphrey, H. C., Santee, M. L., Wu, D. L., Cuddy, D. T., Lay, R. R., Loo, M. S., Perun, V. S., Schwartz, M. J., Stek, P. C., Thurstans, R. P., Boyles, M. A., Chandra, S., Chavez, M. C., Chen, G.-S., Chudasama, B. V., Dodge, R., Fuller, R. A., Girard, M. A., Jiang, J. H., Jiang, Y., Knosp, B. W., LaBelle, R. C., Lam, J. C., Lee, K. A., Miller, D., Oswald, J. E., Patel, N. C., Pukala, D. M., Quintero, O., Scaff, D. M., Snyder, W. V., Tope, M. C., Wagner, P. A., and Walch, M. J.: The Earth Observing System Microwave Limb Sounder (EOS MLS) on the Aura satellite, IEEE Trans. Geosci. Remote Sens., 44, 1106–1121, 2006.

Wright, J. S., Fu, R., Fueglistaler, S., Liu, Y. S., and Zhang, Y.: The influence of summertime convection over Southeast Asia on water vapor in the tropical stratosphere, J. Geophys. Res., 116, D12302, https://doi.org/10.1029/2010JD015416, 2011.